European Journal of Medicinal Chemistry 218 (2021) 113385

Contents lists available at ScienceDirect

European Journal of Medicinal Chemistry

journal homepage: http://www.elsevier.com/locate/ejmech

Novel potent bifunctional carboxylesterase inhibitors based on a polyfluoroalkyl-2-imino-1,3-dione scaffold

Galina F. Makhaeva [a], Sofya V. Lushchekina [a, b], Natalia P. Boltneva [a], Olga G. Serebryakova [a], Nadezhda V. Kovaleva [a], Elena V. Rudakova [a], Natalia A. Elkina [c], Evgeny V. Shchegolkov [c], Yanina V. Burgart [c], Tatyana S. Stupina [d], Alexey A. Terentiev [d], Eugene V. Radchenko [a, e], Vladimir A. Palyulin [a, e], Victor I. Saloutin [c], Sergey O. Bachurin [a], Rudy J. Richardson [f, g, h, *]

[a] Institute of Physiologically Active Compounds Russian Academy of Sciences, Chernogolovka, 142432, Russia
[b] Emanuel Institute of Biochemical Physics Russian Academy of Sciences, Moscow, 119334, Russia
[c] Postovsky Institute of Organic Synthesis, Urals Branch of Russian Academy of Sciences, Ekaterinburg, 620990, Russia
[d] Institute of Problems of Chemical Physics Russian Academy of Sciences, Chernogolovka, 142432, Russia
[e] Department of Chemistry, Lomonosov Moscow State University, Moscow, 119991, Russia
[f] Department of Environmental Health Sciences, University of Michigan, Ann Arbor, MI, 48109, USA
[g] Department of Neurology, University of Michigan, Ann Arbor, MI, 48109, USA
[h] Center of Computational Medicine and Bioinformatics, University of Michigan, Ann Arbor, MI, 48109, USA

ARTICLE INFO

Article history:
Received 28 December 2020
Received in revised form
6 March 2021
Accepted 8 March 2021
Available online 15 March 2021

Keywords:
ADMET
Alkyl 2-arylhydrazinylidene-3-oxo-3-polyfluoroalkylpropionates
Antioxidants
Carboxylesterase
Cholinesterases
Molecular docking

ABSTRACT

An expanded series of alkyl 2-arylhydrazinylidene-3-oxo-3-polyfluoroalkylpropionates (HOPs) **3** was obtained via $Cu(OAc)_2$-catalyzed azo coupling. All were nanomolar inhibitors of carboxylesterase (CES), while moderate or weak inhibitors of acetylcholinesterase and butyrylcholinesterase. Steady-state kinetics studies showed that HOPs **3** are mixed type inhibitors of the three esterases. Molecular docking studies demonstrated that two functional groups in the structure of HOPs, trifluoromethyl ketone (TFK) and ester groups, bind to the CES active site suggesting subsequent reactions: formation of a tetrahedral adduct, and a slow hydrolysis reaction. The results of molecular modeling allowed us to explain some structure-activity relationships of CES inhibition by HOPs **3**: their selectivity toward CES in comparison with cholinesterases and the high selectivity of pentafluoroethyl-substituted HOP **3p** to hCES1 compared to hCES2. All compounds were predicted to have good intestinal absorption and blood-brain barrier permeability, low cardiac toxicity, good lipophilicity and aqueous solubility, and reasonable overall drug-likeness. HOPs with a TFK group and electron-donor substituents in the arylhydrazone moiety were potent antioxidants. All compounds possessed low cytotoxicity and low acute toxicity. Overall, a new promising type of bifunctional CES inhibitors has been found that are able to interact with the active site of the enzyme with the participation of two functional groups. The results indicate that HOPs have the potential to be good candidates as human CES inhibitors for biomedicinal applications.

1. Introduction

In humans and other mammals, carboxylesterases (CESs, EC 3.1.1.1) are important serine esterases that belong to the α/β-hydrolase protein superfamily. CESs, along with CYP450s, are categorized as Phase I enzymes that metabolize drugs and environmental toxicants [1–3]. They are localized in the lumen of the endoplasmic reticulum (ER), and they are responsible for the hydrolytic biotransformation of a wide range of compounds bearing ester, thioester, and amide bonds [4–7]. CESs are important catalysts for the bioactivation of numerous prodrugs and bioinactivation of antedrugs [8,9]. They can also hydrolyze endogenous substrates and play important physiological roles in lipid metabolism and energy homeostasis [10–12].

* Corresponding author. Molecular Simulations Laboratory, Room M6065 SPH-II 2029, University of Michigan, 1415 Washington Heights, Ann Arbor, MI, 48109-2029, USA.
E-mail address: rjrich@umich.edu (R.J. Richardson).

https://doi.org/10.1016/j.ejmech.2021.113385
0223-5234/

Human CESs (hCESs) can be classified into five major families (CES1-CES5) according to the homology of their amino acid sequences [6]. The major carboxylesterase isozymes involved in human drug metabolism are CES1 (hCES1, hCES1A, hCE1) and CES2 (hCES2, hCES2A, hiCE2) [1,4,6,13]. These two enzymes share 47% protein sequence identity, but they exhibit differential tissue distribution as well as distinct substrate and inhibitor specificities [5–7].

Currently, the increased interest in CESs is largely caused by two trends. The first is the extensive use of the ester-containing prodrug concept for improving the absorption and bioavailability of pharmacologically active molecules [8,9,14–16]. The second trend is the ever-increasing amount of information about genetic polymorphisms, various diseases, drug interactions, and xenobiotics that can change CES activity, thus modifying the pharmacokinetics and efficacy of drugs that are CES substrates [8,17–25]. Moderate to high inter-individual variability of hCES1 and hCES2 has been reported from 5- to 160-fold for hCES1, and 4- to 34-fold for hCES2 based on protein abundance, 430-fold based on mRNA level, and 127-fold based on hydrolytic activity [9]. Additional interest in CESs is connected with recently increasing data on their participation in the metabolism of cholesteryl esters, triacylglycerols, and other endogenous lipids; thus, CESs can serve as therapeutic targets for the treatment of a variety of human metabolic disorders [10,11,26–28].

The importance of CES in both human health and drug metabolism has aroused great interest in the discovery of potent CES modulators, e.g., potent and selective inhibitors of hCES1 and hCES2. Inhibitors of CESs could be used as co-drugs to improve pharmacokinetics, efficacy, and safety profiles of clinically approved drugs for which CESs are involved in their metabolism and clearance [2,29–32]. Because of the critical role of hCES1 in metabolizing cholesteryl esters, inhibitors of hCES1 have the potential to treat hypertriglyceridemia, obesity, type 2 diabetes, and atherosclerosis [33].

The main classes of compounds among which effective and selective CES inhibitors have been found include *bis*-arylsulfonamides [34], 1,2-diones including benzil and its analogs [35], alkyl-1,2-diones [36], isatins [37], and 1,2-quinones [35], as well as natural compounds such as tanshinones [38,39], and β-lapachones [40] containing a 1,2-dione moiety (Fig. 1). Trifluoromethyl ketone (TFK) derivatives [41] are also highly active reversible inhibitors of CES. Selective CES covalent inhibitors with low acute toxicity have been found among carbamates. They include *O*-carbamoylated 1-hexafluoroisopropanols, discovered by our group [42], and carbamates WWL113 and WWL229, selectively inhibiting mouse Ces3, which is a human CES1 ortholog, found by Cravatt's group [43].

Compounds with a 1,2-dione scaffold (Fig. 1) have been identified as the most important structures for CES inhibition. These compounds have K_i values in the nanomolar range and exert potent and selective inhibitory effects toward hCES1 or hCES2 depending on the orientation of the dione oxygens [35,39,44,45]. While the 1,2-dione moiety is very beneficial for CES inhibition [39,40], such compounds do not exhibit untoward inhibitory effects on human acetylcholinesterase (AChE, EC 3.1.1.7) or butyrylcholinesterase (BChE, EC 3.1.1.8) [2,33].

TFK (Fig. 1) are some of the most potent CES inhibitors identified to date with K_i values in the low nanomolar range, and these compounds mostly demonstrated poor specificity toward hCES1 or hCES2 [46]. TFK chemotype is very efficient at inhibiting many enzymes whose catalytic mechanism involves attack by a nucleophilic catalytic residue e.g., serine. The extreme inhibitor potency of this type of compounds is attributed to the polarization of a carbonyl by the trifluoromethyl group, which greatly increases the electrophilicity of the carbonyl carbon and hence its susceptibility to nucleophilic attack [41,47]. The recent QM/MM study demonstrated that such reaction with AChE occurs almost without energy barrier [48]. The mechanism of inhibition of esterases by TFK compounds is associated with formation of so-called transition state analogs [35,49], as was shown in an X-ray study of AChE inhibition by TFK [50], although this type of adduct is more correctly termed as a "tetrahedral intermediate analog" [51,52].

Recently, our team developed a new polyfluoroalkyl-2-imino-1,3-dione scaffold that combines in one molecule two chemotypes – TFK and 1,2-dione – specific for effective CES inhibition [53–56]. Its distinguishing feature is the replacement of one carbonyl function in the 1,2-dione fragment by a bioisosteric imino group, which can be chemically modified. We first discovered that alkyl 2-arylhydrazinylidene-3-oxo-3-polyfluoroalkylpropionates (Fig. 2, HOP) showed the ability to inhibit porcine liver CES in the nanomolar range, with significantly lower activity against two related enzymes, AChE and BChE [53]. Effective and highly selective CES inhibitors have also been found among HOP analogs bearing natural alcohol moieties (HOP^N) [56] or an acid residue (HOA) [57] as well as their cyclic derivatives, 7-hydroxy-7-polyfluoroalkyl-4,7-dihydroazolo[5,1-*c*][1,2,4]triazines [58] (Fig. 2). An additional

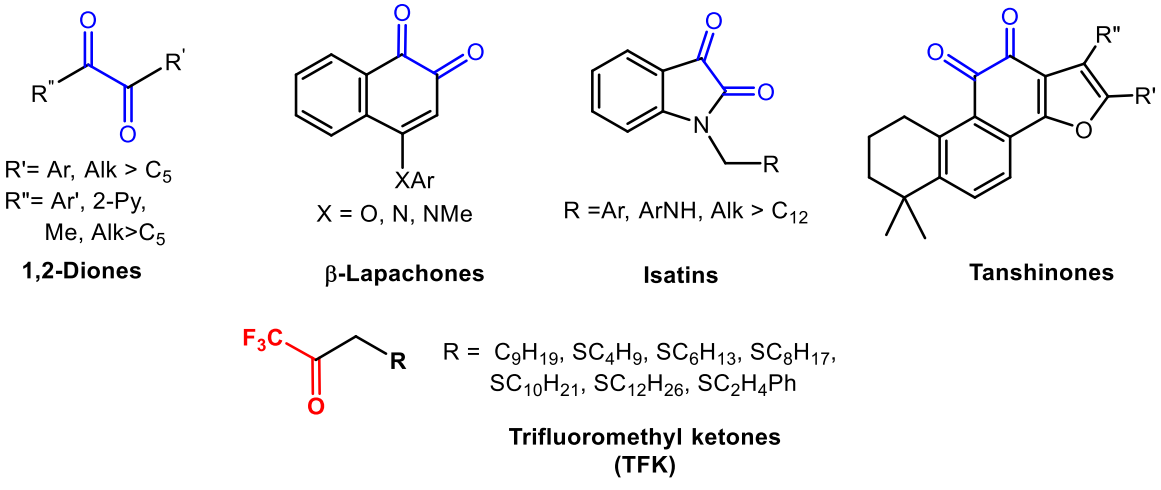

Fig. 1. CES inhibitors having 1,2-dione and TFK scaffolds.

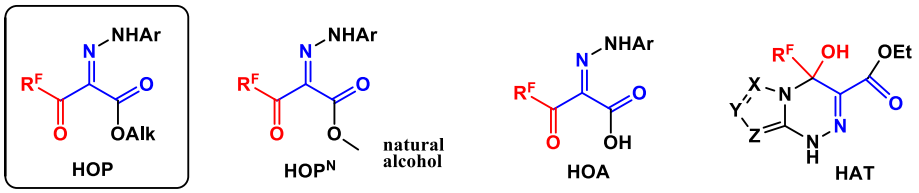

Fig. 2. New CES inhibitors based on the 2-imino-3-polyfluoroalkyl-1,3-dione scaffold.

property of all compounds with the 2-imino-1,3-dione scaffold is their high radical-scavenging activity [56–58], which we regard as a positive attribute for the potential medicinal use of these molecules.

The aim of the present study was to elucidate the unique features of compounds containing the polyfluoroalkyl-2-imino-1,3-dione scaffold that give rise to their high activity and selectivity toward CES compared to cholinesterases. We accomplished this goal by first synthesizing an expanded series of the most active HOPs using a more productive synthetic protocol than we had used previously. Next, we performed a biological evaluation of the compounds as inhibitors of porcine liver CES along with human erythrocyte AChE and equine serum BChE accompanied by molecular docking. Some of the compounds were also studied as inhibitors of human CES1 and CES2. Additionally, to assess potential pharmacokinetic properties of HOPs, we determined their ADMET profiles computationally and assessed their antioxidant activity by the ABTS assay as an indicator of their potential hepatoprotective effect. Finally, we determined the cytotoxicity of the compounds *in vitro* with the MTT assay in human FetMSC cells and assessed their acute toxicity *in vivo* in mice.

2. Results and discussion

2.1. Chemistry

To synthesize 2-arylhydrazinylidene-3-oxo esters, the commonly used procedure is azo coupling of 3-oxo esters **1** with aryldiazonium salts **2**, which are obtained from reacting the arylamine with sodium nitrite in aqueous HCl [59]. The usual medium for azo coupling is a water-miscible organic solvent and water with sodium acetate or sodium hydroxide for enolate generation [60]. However, the reaction under these conditions can be complicated by Japp-Klingemann cleavage or formazan formation. Recently, it has been proposed to use mechanically activated solid-state synthesis of arylhydrazone derivatives via a high-speed ball mill in the absence of solvent [61]. It has also been reported that $Sc(OTf)_3$ could be used to catalyze transfer diazenylation of 1,3-dicarbonyls with aryltriazenes through N–N bond cleavage [62]. To increase the yield of target arylhydrazones, we have carried out azo coupling in a water-chlorohydrocarbon medium in the presence of tetraalkylammonium halide as a phase-transfer catalyst [53].

To synthesize alkyl 2-arylhydrazinylidene-3-oxo-3-polyfluoroalkylpropionates **3** (HOPs), we decided to apply $Cu(OAc)_2$-catalyzed azo coupling of 3-oxo esters **1a-h** with various aryldiazonium salts **2a-i** in a mixture of acetone-water. Using this protocol, we obtained a large number of esters **3a-s** with high yields (Scheme 1A). The same method was used for synthesis of non-fluorinated analog **3t**. Copper (II) acetate was not only a catalyst, but also it served as a reagent to bind 3-oxo esters **1** into copper complexes, which were less prone to undergo cleavage. To obtain trifluoromethyl-containing 2-tolylhydrazinylidene-1,3-diketones **5a,b**, azo coupling of tolyldiazonium salt **2b** was carried out with lithium 1,3-diketonates **4a,b**, which were the intermediates in a Claisen condensation of esters with methyl ketones under lithium hydride action to yield 1,3-diketone reagents [63] (see Scheme 1B).

The use of these techniques was more efficient than previous ones [64–66], because the yields of targeted arylhydrazones **3** and **5** reached 87%. Moreover, the synthesized compounds did not need additional purification owing to the absence of side reactions under the conditions of synthesis.

QM calculations demonstrated that for HOPs **3**, the *Z*-isomer is more stable than the *E*-form, in which the polyfluoroacyl oxygen atom is involved in an intramolecular hydrogen bond (Fig. 3, Table 1). For example, the energy difference was 3.5 kcal/mol for compound **3k** (Fig. 3). For the *Z*-isomer, there is also the possibility of formation of a hydrogen bond between the NH-group of the arylhydrazone fragment and the oxygen atom of the ester alkoxy group, but such a conformation was less favorable (5.5 kcal/mol difference for compound **3k**) when the compounds were not bound to the enzyme active site.

These QM calculation results were in good agreement with our previous experimental findings [67]. According to ^{1}H, ^{19}F and ^{13}C NMR spectroscopy and X-ray diffraction analysis, both in the solid state and in $(CD_3)_2CO$ or $CDCl_3$ solution, HOPs **3** exist as *Z*-isomers. Similar results were obtained in our previous study of $HOPs^N$ bearing higher or natural alcohol moieties [56] (Scheme 2).

We also defined the conformational form of 2-arylhydrazinylidene-3-oxo esters **3** in aqueous DMSO. According to ^{1}H and ^{19}F NMR spectroscopy, all esters **3a-s** containing a polyfluoroalkyl substituent exist only as the *Z*-isomer in DMSO-d_6. In contrast to compounds **3a-s,** the non-fluorinated analog **3t** is a mixture of *Z*- and *E*-isomers in these solutions (Scheme 2, see Experimental).

2.2. Inhibition studies of CES, AChE and BChE: structure-activity relationships

The inhibitory potency of our synthesized compounds against CES and structurally related cholinesterases (i.e., their esterase profile) was determined using commercially available enzymes: porcine liver CES, human erythrocyte AChE, and equine serum BChE (Sigma, USA). AChE from human erythrocytes was used along with two enzymes of non-human origin, because of their relatively low cost and the exploratory character of this work. High protein sequence identities between human and equine BChE (90%) and human CES1 and porcine liver CES (77%) [68] along with our previous results [68–70] supported the applicability of this set of enzymes for determining esterase profiles of new compounds.

Data characterizing the esterase profile of compounds **3** and **5** are shown in Table 2. All compounds were moderate or weak inhibitors of cholinesterases. At the same time, all HOPs **3a-m** containing the TFK fragment were highly effective inhibitors of CES with IC_{50} values in the nanomolar range. Moreover, the variation of substituent in the arylhydrazone moiety did not substantially affect the inhibitory activity of these compounds, with the exception of compounds **3h,i,** where a decrease in activity may be associated with steric hindrance.

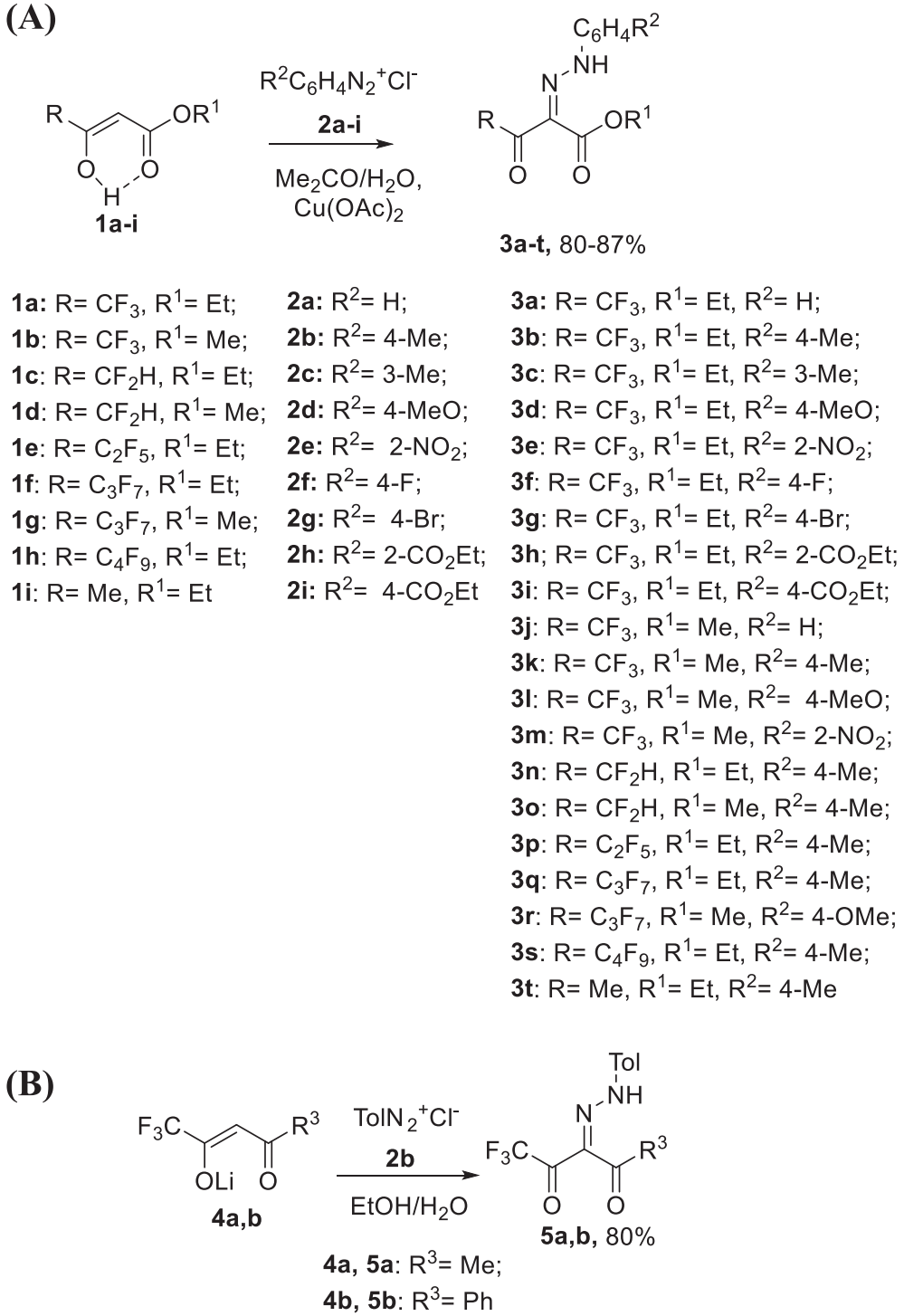

Scheme 1. Synthesis of 2-arylhydrazinylidene-3-oxo esters **3** (A) and 2-arylhydrazinylidene-1,3-diketones **5** (B).

HOPs **3a-m** contain two functional groups with a polarized carbonyl in their structure: a TFK moiety and an ester moiety; both of them could react with the active site serine and thus affect the inhibitory potency against serine esterases.

To clarify the role of the TFK group, the inhibitory activity of oxo esters **3** in which the CF_3 group was replaced by CHF_2 (**3n,o**) and CH_3 (**3t**) was studied. It turned out that replacing CF_3 (**3b,k**) with CHF_2 (**3n,o**) led correspondingly to about a 400-fold (**3b** vs **3n**) to100-fold (**3k** vs **3o**) decrease in anti-CES activity, with almost complete disappearance of AChE and BChE inhibition. Upon replacing the CF_3 group (**3b**) by CH_3 (**3t**), inhibitory activity against CES also dramatically decreased (from IC_{50} = 7.41 nM for **3b** to 12.1% inhibition at 20 μM for **3t**). Thus, the results indicate the importance of the TFK moiety, $CF_3C(O)$, for potent action of HOPs **3** against the studied esterases, especially CES. The weakening of the inhibitory activity of esters having CHF_2 (**3n,o**) and CH_3 (**3t**), could be due to a decrease in δ+ on the carbon atom of the acyl moiety, which is involved in binding to the active site of CES. Another

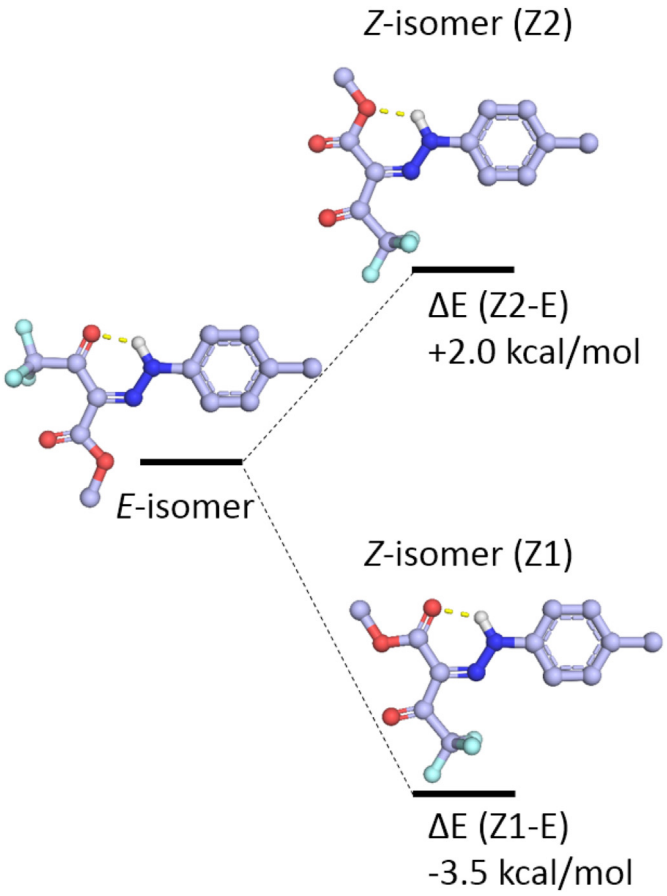

Fig. 3. Energy diagram of the *E*-isomer and two conformers of the *Z*-isomer for compound **3k**. Two possible conformations of the *Z*-isomer have intramolecular hydrogen bonds with the carbonyl oxygen (Z1) and the oxygen atom of the ester alkoxy group (Z2).

Table 1
Energy differences of the two conformers of the *Z*-isomers relative to *E*-isomer energy level for HOPs 3.

Compound	ΔE, kcal/mol	
	Z1-E	Z2-E
3a	−3.7	2.1
3b	−3.6	2.1
3c	−3.6	2.1
3d	−3.5	2.3
3e	−3.7	−1.1
3f	−3.6	2.2
3g	−3.7	2.1
3h	−2.5	3.3
3i	−3.8	2.0
3j	−3.8	1.7
3k	−3.5	2.0
3l	−3.7	1.9
3m	−3.9	−1.3
3n	−3.1	2.5
3o	−1.5	4.1
3p	−3.0	2.7
3q	−2.3	3.0
3r	−2.4	3.2
3s	−0.1	5.4
3t	−0.8	5.0

decrease in HOP anti-CES activity, although less appreciable, occurred with increasing the length of the CF_3 group to C_2F_5 (**3p**), C_3F_7 (**3q,r**) and C_4F_9 (**3s**). This decrease of inhibitory activity with increasing polyfluoroalkyl chain length appeared to be caused by both electronic and steric factors.

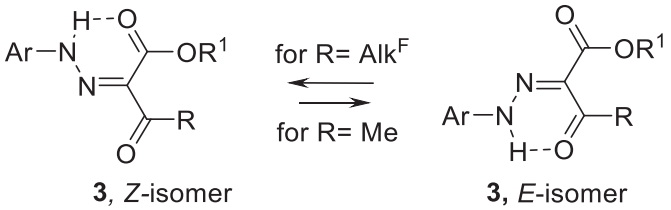

Scheme 2. The geometrical isomerism of alkyl 2-arylhydrazinylidene-3-oxo esters **3**.

Interestingly, most of the HOP Me esters were 4–9 times less effective against CES than the corresponding Et esters, except Me and Et esters **3e,m** having a 4-NO_2 group in the arylhydrazone moiety that displayed the same high anti-CES activity (Table 2).

To elucidate the role of the ester moiety in the anti-CES efficiency of HOPs **3**, we replaced the ester group with two different keto groups – MeC(O) and PhC(O) – 1,3-diketones **5a** and **5b**. The results provided evidence for the large contribution of the ester moiety to anti-CES activity: substitution with PhC(O) (**5b**) reduced anti-CES activity about 700 times compared to the Et ester **3b** and about 200 times compared to Me ester **3k**. Moreover, substitution with MeC(O) (**5a**) reduced inhibitor potency by another order of magnitude (Table 2). Diketones **5a** and **5b** were also very weak inhibitors of cholinesterases.

Thus, in order to exhibit maximum anti-CES activity, a molecule based on the polyfluoroalkyl-2-imino-1,3-dione scaffold should contain a combination of TFK and an ester group, with the Et esters preferable.

2.3. Kinetics studies of porcine CES, human AChE, and equine BChE inhibition

The compound **3k** was selected for a steady-state kinetics study of inhibition toward porcine CES, human AChE, and equine BChE. Graphical analysis of steady-state inhibition kinetics data for oxo ester **3k** against the three esterases is shown in Fig. 4. Binding of **3k** to all three enzymes changed both V_{max} and K_m values. Such alterations are consistent with mixed-type inhibition of all three esterases, with K_i = 14.0 ± 1.1 nM (competitive component) and αK_i = 82.2 ± 5.7 nM (noncompetitive component) for CES. The corresponding constants for AChE were K_i = 10100 ± 800 nM and αKi = 139000 ± 11000 nM, and for BChE were K_i = 29200 ± 2300 nM and αK_i = 72700 ± 5100 nM.

2.4. Inhibition study of human CES1 and CES2. Structure-activity relationships

All studied HOPs **3** showed high activity and selectivity against porcine CES compared to cholinesterases. Among these, potent and selective compounds were studied as inhibitors of the main human isoenzymes involved in biotransformation of ester-containing drugs, human CES1 and CES2. Data on the inhibitory activity of these compounds toward hCES1 and hCES2 are presented in Table 3.

As can be seen from Table 3, most studied CES inhibitors showed higher selectivity for hCES1. Analysis of data on inhibition of human CES isoenzymes revealed that electron donor substituents in the arylhydrazone moiety, such as Me, OMe (Et esters **3b, 3c**, **3d** and Me esters **3k**, **3l**) improved CES1 inhibitory activity and selectivity, while compounds with electron-withdrawing substituents NO_2, F (Et esters **3e**, **3f** and Me ester **3m**) were more active against CES2. Oxo esters **3a,j** having a

Table 2
Esterase profiles and $ABTS^{\cdot+}$-scavenging activity of HOPs **3** and diketones **5**.

No.	Compound			Inhibitory activity IC_{50} ± SEM (nM) or inhibition % at 20 μM.			$ABTS^{\cdot+}$-scavenging	
	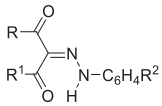							
	R	R^1	R^2	Porcine CES	Human AChE	Equine BChE	TEAC[a]	IC_{50}, μM
3a	CF_3	OEt	H	6.14 ± 0.55	3220 ± 280	8420 ± 720	0.80 ± 0.04	26.7 ± 1.2
3b	CF_3	OEt	4-Me	7.41 ± 0.58	7320 ± 580	8340 ± 660	0.95 ± 0.05	21.4 ± 0.9
3c	CF_3	OEt	3-Me	7.27 ± 0.58	30400 ± 2100	38100 ± 2900	0.85 ± 0.04	25.4 ± 1.1
3d	CF_3	OEt	4-OMe	13.1 ± 1.0	4620 ± 410	24.3 ± 1.9%	1.0 ± 0.04	19.3 ± 0.5
3e	CF_3	OEt	2-NO_2	4.95 ± 0.39	759 ± 61	8060 ± 640	0.04 ± 0.01	n.d.
3f	CF_3	OEt	4-F	7.16 ± 0.57	2670 ± 210	11300 ± 900	0.60 ± 0.04	35.3 ± 1.4
3g	CF_3	OEt	4-Br	5.14 ± 0.41	1360 ± 110	2020 ± 140	0.53 ± 0.03	36.3 ± 1.5
3h	CF_3	OEt	2-CO_2Et	41.6 ± 3.3	481 ± 38	122 ± 7	0.04 ± 0.01	n.d.
3i	CF_3	OEt	4-CO_2Et	47.1 ± 3.2	3790 ± 260	19600 ± 1600	0.1 ± 0.01	193 ± 2.6
3j	CF_3	OMe	H	55.5 ± 4.4	20100 ± 1600	14500 ± 1100	0.78 ± 0.04	26.6 ± 1.3
3k	CF_3	OMe	4-Me	27.8 ± 2.5	28300 ± 2200	33000 ± 2300	0.98 ± 0.03	21.2 ± 0.9
3l	CF_3	OMe	4-OMe	46.7 ± 3.2	30300 ± 2400	49600 ± 3900	0.97 ± 0.05	22.5 ± 1.1
3m	CF_3	OMe	2-NO_2	7.65 ± 0.68	20900 ± 1800	45100 ± 4100	0.03 ± 0.01	n.d.
3n	CF_2H	OEt	4-Me	3230 ± 280	18.2 ± 1.4%	12.4 ± 1.9%	0.37 ± 0.02	53.3 ± 2.1
3o	CF_2H	OMe	4-Me	1570 ± 120	5.8 ± 1.1%	2.3 ± 0.5%	0.38 ± 0.02	52.6 ± 2.5
3p	C_2F_5	OEt	4-Me	164 ± 11	11.5 ± 1.9%	31100 ± 2100	0.36 ± 0.02	55.2 ± 2.1
3q	C_3F_7	OEt	4-Me	102 ± 8	23.6 ± 2.1%	42100 ± 3700	0.30 ± 0.02	62.3 ± 1.8
3r	C_3F_7	OMe	4-OMe	103 ± 9	7.1 ± 1.3%	21.2 ± 1.9%	0.40 ± 0.03	50.3 ± 2.1
3s	C_4F_9	OEt	4-Me	89.3 ± 4.2	17.2 ± 1.5%	4.0 ± 1.1%	0.26 ± 0.02	66.6 ± 2.5
3t	Me	OEt	4-Me	12.1 ± 1.8%	6.8 ± 1.2%	n.a.	0.38 ± 0.03	52.4 ± 1.8
5a	CF_3	Me	4-Me	56600 ± 5100	11.0 ± 1.9%	13.4 ± 2.3%	1.33 ± 0.2	15.6 ± 0.9
5b	CF_3	Ph	4-Me	5540 ± 440	9.1 ± 1.7%	19.4 ± 1.6%	1.7 ± 0.18	12.8 ± 0.5
BNPP				1800 ± 110	n.a.	n.a.	n.d.	n.d.
Trolox				n.d.	n.d.	n.d.	1.0	20.4 ± 0.6
Ascorbic acid				n.d.	n.d.	n.d.	0.98 ± 0.03	21.6 ± 1.2
Catechol				n.d.	n.d.	n.d.	1.2 ± 0.04	16.4 ± 0.9

Data are expressed as mean ± SEM, $n = 3$.
Esterase profiles: n.a. = not active at 20 μM.
Values expressed as % correspond to % inhibition at 20 μM.
Values without units of measurement correspond to IC_{50} values in nM.
n.d. = not determined.
[a] TEAC (Trolox equivalent antioxidant capacity) was determined from the ratio of the slopes of the concentration-response curves test compound/Trolox.

phenylhydrazone substituent ($R^2 = H$) displayed the same degree of inhibition of human CES1 and CES2.

For compounds with longer fluorinated substituents, the replacement of CF_3 with C_2F_5 (**3p**) and C_3F_7 (**3r**) led to decreasing inhibitory activity against both human CES isoenzymes (compare IC_{50} **3p** and **3b**; **3r** and **3l**), but at the same time, selectivity toward hCES1 was maintained at a similar level as that of the CF_3 derivatives. It may reasonably be assumed that hCES1 selectivity is determined by the presence of the electron-donating Me or MeO substituent in the arylhydrazone moiety.

2.5. Molecular modeling

To gain insight into the structural aspects for the high efficiency and selectivity of HOPs toward CES, we performed molecular docking studies of HOPs interactions with CES, AChE, and BChE. X-ray crystal structures of the human enzymes were used.

Molecular docking of the *Z*-isomers of HOPs **3a-m** into the CES active site revealed two major clusters of binding poses suggesting further reaction: one cluster with the TFK group in the active site (Fig. 5A and B) and the other with the ester group in the active site (Fig. 5C and D). For each of the two clusters, there were two possible orientations of the ligands with respect to the catalytic residues. Thus, there were four major binding positions for compounds in the CES catalytic site.

For the TFK group in the active site, the entire molecule could be flipped by 180°, such that the $-CF_3$ group was directed either toward the catalytic histidine or away from it (Fig. 5A and B). In both cases, the position of the TFK-group in the active site was such that the carbonyl oxygen atom was in the oxyanion hole and the carbonyl carbon atom was facing the catalytic serine. Such a position would favor a subsequent covalent interaction with the formation of a hemiketal. Moreover, the position of the TFK group shown in Fig. 5B also had an additional hydrogen bond between the NH-group of Gly142 in the oxyanion hole and the oxygen atom of the ester alkoxy group.

When the ester group was in the active site, the poses again differed by a 180° flip of the TFK-arylhydrazone fragment, while the position of the ester group itself remained the same (Fig. 5C and D). Both configurations suggest the possibility of subsequent hydrolysis of this group, followed by reinhibition of the enzyme by the product [57].

Estimates of docked free energies for all four types of binding poses were very close, within 0.5 kcal/mol, which is less than the AutoDock standard deviation of 2.5 kcal/mol [71].

Such binding to the CES active site is associated with the loss of the inherent planarity of aromatic system found in the free compounds and, in the case of binding of the ester group in the active site, there is impairment of intramolecular hydrogen bonding. However, these destabilizations of the ligands are compensated by their specific interactions with the enzyme, and subsequent reactions would explain the high inhibitory activity of the compounds toward CES.

Molecular docking also showed strong additional binding of compounds **3e** and **3m** in the CES active site, consisting of binding

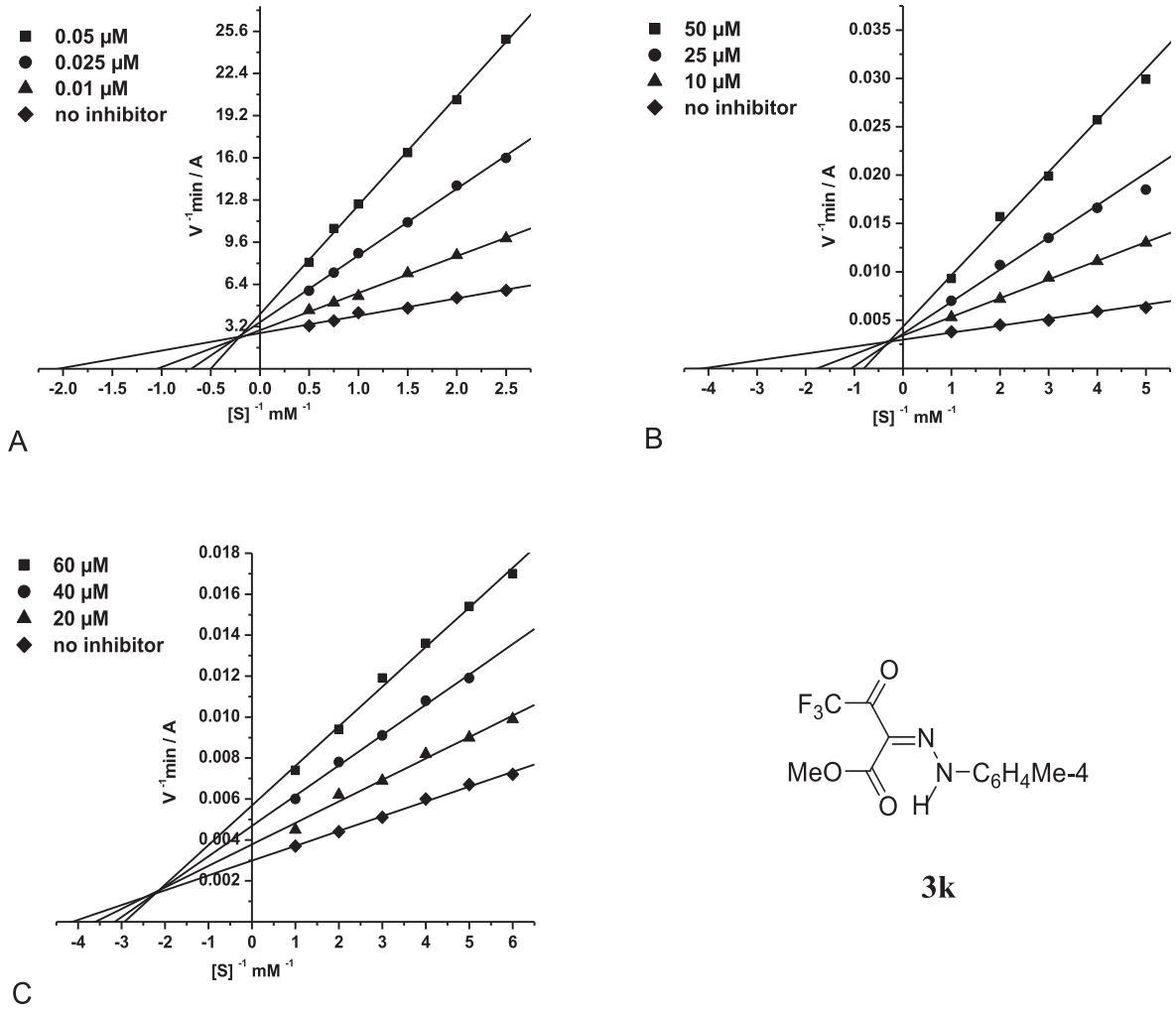

Fig. 4. Steady state inhibition of (**A**) porcine liver CES, (**B**) AChE from human erythrocytes, (**C**) BChE from equine serum by oxo ester **3k**. Lineweaver-Burk double-reciprocal plots of initial velocity and substrate concentrations in the presence of inhibitor (three concentrations) and without inhibitor are presented. [S], mM − concentration of substrates; V − initial velocity rate; A − absorbance.

Table 3
Inhibitory activity of HOPs **3** against hCES1 and hCES2.

No.	Compound			IC_{50} (nM) ± SEM		Selectivity Ratio
	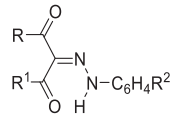					
	R	R^1	R^2	hCES1	hCES2	IC_{50}(hCES2)/IC_{50}(hCES1)
3a	CF_3	OEt	H	6.10 ± 0.48	4.33 ± 0.38	0.70
3b	CF_3	OEt	4-Me	2.92 ± 0.23	72.31 ± 5.12	24.7
3c	CF_3	OEt	3-Me	5.17 ± 0.47	23.44 ± 1.61	4.5
3d	CF_3	OEt	4-OMe	4.29 ± 0.34	70.51 ± 6.33	16.4
3e	CF_3	OEt	2-NO_2	24.12 ± 2.11	4.04 ± 0.28	0.17
3f	CF_3	OEt	4-F	22.31 ± 1.72	9.84 ± 0.78	0.44
3g	CF_3	OEt	4-Br	15.32 ± 1.14	10.81 ± 0.83	0.71
3j	CF_3	OMe	H	11.54 ± 0.93	47.74 ± 3.82	4.1
3k	CF_3	OMe	4-Me	16.33 ± 1.31	193.34 ± 15.18	11.8
3l	CF_3	OMe	4-OMe	21.31 ± 1.42	339.25 ± 30.32	15.9
3m	CF_3	OMe	2-NO_2	102.34 ± 8.4	16.92 ± 1.34	0.17
3p	C_2F_5	OEt	4-Me	47.42 ± 4.21	610.24 ± 54.12	33.9
3r	C_3F_7	OMe	4-OMe	111.28 ± 8.33	230.09 ± 18.21	11.1

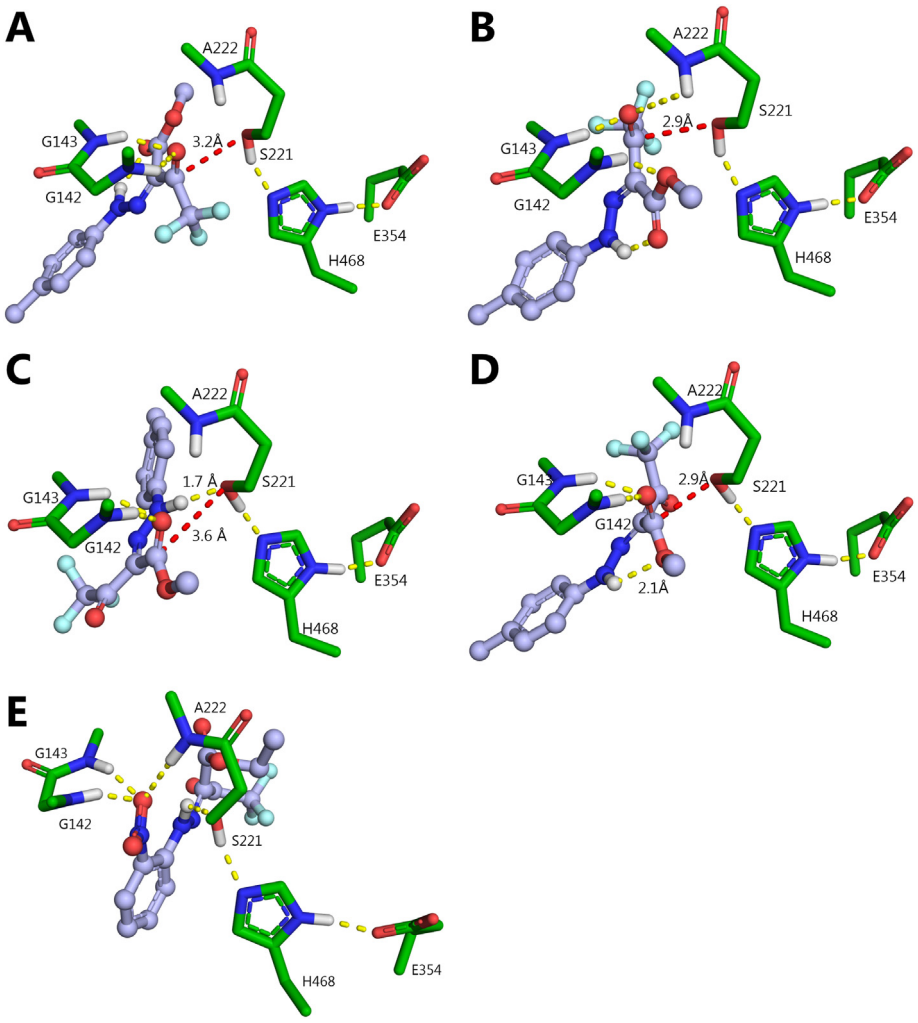

Fig. 5. Binding poses of compounds (with compound **3k** shown as an example) to hCES1: A and B — two different orientations of the TFK group in the active site; C and D — ester group in the active site with different orientations of the remainder of the molecule, the TFK-arylhydrazone fragment. E – compound **3m** pose with the nitro group in the active site. Yellow dashes show hydrogen bonds, whereas red dashes indicate directions of potential subsequent nucleophilic attack. Carbon atoms of enzyme residues are colored green; ligand carbons are colored light blue; fluorine atoms are colored cyan. Nitrogen = blue; oxygen = red. When hydrogens are included, they are colored white.

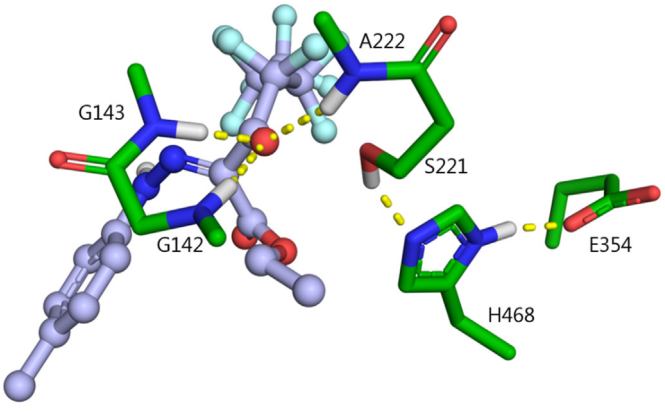

Fig. 6. Binding pose of compound **3s** ($R^F = C_4F_9$) in the CES with the polyfluoroalkyl keto group in the active site. Protein residue carbons = green; ligand carbons = light blue; nitrogens = blue; oxygens = red; fluorines = cyan; when hydrogens are depicted, they are colored white. Yellow dashed lines = hydrogen bonds.

of the NO_2 group to the oxyanion hole (Fig. 5E). Such a binding pose does not suggest further covalent interactions; however, the spacious CES active site could allow reorientation of the ligand to one of the reactive positions.

Increasing the length of the fluorinated substituent made the reactive position of the polyfluoroalkyl keto group in the CES active site less favorable due to steric conflicts with surrounding residues. As shown in Fig. 6 for compound **3s** ($R^F = C_4F_9$), the carbonyl atom is displaced from a reactive position in the active site. These results explain why $R^F = CF_3$ is optimal for maximum anti-CES inhibitor activity, whereas compounds with longer polyfluoroalkyl groups were 10–20 times less potent (Table 2).

Differences in binding modes of HOPs **3** to CES, AChE, and BChE active sites determine the reasons for their selectivity. The large CES1 active site (~1300 $Å^3$) is lined predominately by hydrophobic amino acids with aliphatic chains, allowing the entry of numerous structurally diverse substrates [32].

Due to differences in their active site shape and size compared to CES, the cholinesterases exhibited less diversity in their inhibitor binding poses than was seen with CES. Moreover, whereas AChE had binding poses of HOP **3k** in both the gorge and active site, poses in the active site did not suggest the possibility of a subsequent covalent reaction (Fig. 7A). BChE had only one potentially reactive orientation of **3k** with the TFK group in the active site. A specific

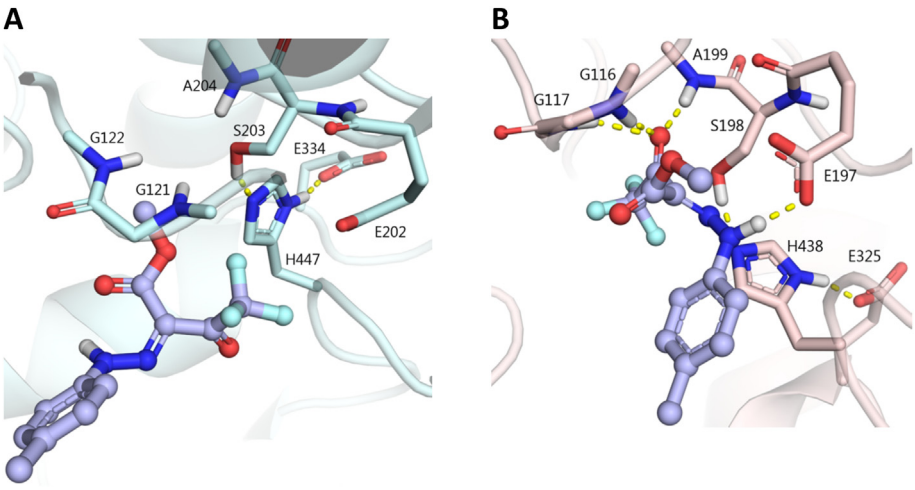

Fig. 7. Example of binding of HOP **3** to cholinesterases: (A) compound **3k** in the active site of AChE; (B) **3k** in the active site of BChE. Nitrogens = blue; oxygens = red; AChE residue carbons = light cyan, BChE residue carbons = light pink; ligand carbons = light blue; fluorines = cyan; when hydrogens are depicted, they are colored white.

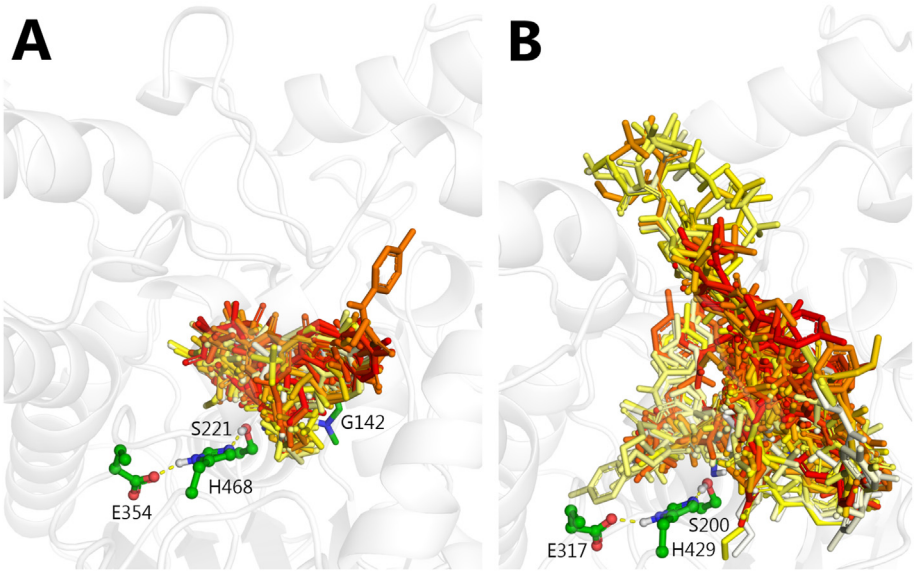

Fig. 8. All binding poses obtained by molecular docking of compound **3p** to CES1 (A) and CES2 (B). Ligand poses are colored according to estimated binding affinity increasing from white to red. Protein residue colors: carbon = green; nitrogen = blue; oxygen = red; hydrogen = white.

feature of this binding was a hydrogen bond between the arylhydrazone fragment NH-group of **3k** and Ser198 (Fig. 7B). However, a hydrogen bond of this fragment with the active site Glu197 could prevent a chemical reaction, and unlike CES, the BChE active site did not allow reorientation of the **3k** molecule to a more reactive position. In addition, such binding was associated with a more pronounced loss of planarity in the conjugated arylhydrazone group than was the case with CES, which makes a reactive position less favorable. These observations serve to explain the reduced efficiency of HOP **3** against cholinesterases compared to CES.

Molecular modeling also allowed us to see differences in the binding of pentafluoroethyl-substituted HOP **3p** that correlated with the highest selectivity between human CES isoenzymes: IC_{50}CES2/IC_{50}CES1 = 33.9 (Table 3). In docking compound **3p** to CES1, active site poses were most prevalent (Fig. 8A), while docking **3p** to the CES2 homology model resulted in much more diverse binding poses mostly outside of the active site (Fig. 8B).

2.6. Antioxidant activity

CES and cytochromes P450 are enzymes of phase I metabolism of xenobiotics [72,73] and have close localization in hepatocytes. In this regard, a potentially useful additional property of CES inhibitors could be their antioxidant action [56], which can protect the liver from damage caused by highly reactive metabolites arising from the biotransformation of drugs under the action of the cytochrome P450 microsomal enzyme system [74,75].

The antioxidant activity of compounds **3** and **5** was evaluated in the ABTS radical cation ($ABTS^{\bullet+}$) scavenging assay [76], using Trolox as the reference antioxidant. As shown in Table 1, the $ABTS^{\bullet+}$-scavenging activity of the tested HOPs **3** containing a trifluoromethyl group depended on the substituent in the arylhydrazone moiety. Compounds **3b-d,k,l** with electron-donor Me or MeO substituents had a high antiradical activity comparable to that of Trolox (TEAC range, 0.85–1.0), ascorbic acid, and catechol, and

similar to that of earlier studied analogs – HOP^N containing various fragments of higher or natural alcohols [56]. The oxo esters **3a,j** having a non-substituted phenylhydrazone moiety also revealed good radical-scavenging action (TEAC 0.78–0.8). The $ABTS^{\bullet+}$-scavenging activity decreased for compounds with electron-withdrawing substituents **3f** (*p*-F, TEAC = 0.6), **3g** (*p*-Br, TEAC = 0.53), with the lowest values for compounds **3i** (*p*-CO_2Et, TEAC = 0.1), **3e, 3h** and **3m** (*o*-NO_2, *o*-CO_2Et, TEAC = 0.03–0.04).

Replacement of the trifluoromethyl group (**3b**, TEAC = 0.95) with CHF_2 (**3n,** TEAC = 0.37) and CH_3 (**3t**, TEAC = 0.38) as well as elongation of the polyfluoroalkyl group (**3p** – C_2F_5, **3q** – C_3F_7, **3s** – C_4F_9) decreased radical-scavenging activity (TEAC = 0.36, 0.30, 0.26, respectively). Similar data were obtained for Me esters: **3k** (CF_3, TEAC = 0.98) *vs* **3o** (CHF_2, TEAC = 0.38) and **3r** (C_3F_7, TEAC = 0.4). Thus, the presence of a trifluoromethyl group in the oxo esters **3** along with an electron-donor substituent in the arylhydrazone moiety were the optimal conditions for high radical-scavenging activity.

The most active scavengers of free radicals among the studied compounds were 2-arylhydrazylidene-1,3-diketones **5a,b** in which the ester fragment was replaced with a ketone. Furthermore, a diketone with a benzoyl moiety **5b** (TEAC = 1.7) was more effective than the acyl-containing analog **5a** (TEAC = 1.33).

The calculated HOMO/LUMO gap values (DFT (B3LYP)/6-31++G** method) for compounds **3h** (3.89 eV), **3k** (3.77 eV) and **5b** (3.60 eV) agreed with increasing antioxidant activity in this series (TEAC values **3h** < **3k** < **5b**, Table 2).

2.7. Cytotoxicity studies and acute toxicity evaluation

Cell viability was assessed using the MTT assay. All studied HOPs **3a-c,e-g,o** were found to have relatively low potency against human FetMSC cells in the MTT assay, with IC_{50} values exceeding 500 μM (Table 4). Higher concentrations were not used because of the limited solubility of compounds.

The acute toxicity of some of the most active compounds **3a-c,e,g,m** was estimated in CD-1 mice. The tested compounds in 2% (w/v) starch mucilage solution were injected intraperitoneally. Animals were observed for lethality during 14 days. The obtained preliminary data (Table 4) allowed us to conclude that LD_{50} values for these compounds were expected to exceed 300 mg/kg, because after administering this dose none of the animals died. Increasing the dose of **3a** to 600 mg/kg and **3b** to 900 mg/kg did not lead to the death of any animals in the experiment.

Although the limited solubility of the compounds has prevented the exact cytotoxicity and acute toxicity measurements, it should be stressed that their inhibitory concentrations are at least several orders of magnitude lower, ensuring extremely wide safety margins.

2.8. Predicted ADMET and physicochemical profiles

The results of the computational estimation of a number of ADMET properties for HOPs **3** are shown in Table 5. As can be seen, all the compounds had predicted high values for intestinal absorption, enabling their oral administration. The majority of the compounds was predicted to have good blood-brain barrier permeability (brain concentration is about 70–165% of the plasma concentration), ensuring very efficient action on the CNS, although the permeability of compounds **3e** and **3m** may be more moderate (brain concentration about 40% of the plasma concentration). Both parameters of the cardiac toxicity risk (pK_i and pIC_{50}) for all analyzed compounds (3.8–5.6 log units) were in the lower part of their possible range (3–9 log units). The predicted lipophilicities and aqueous solubilities of the compounds were also good, although some improvement would be desirable for a few compounds. Finally, the integral quantitative estimates of drug-likeness (QED) values for most of the compounds were close to 0.4. Thus, the predicted ADMET properties of compounds **3** were quite acceptable for potential lead compounds at the early drug development stages.

2.9. PAINS analysis

The Pan Assay INterference compoundS (PAINS) filter check for the compounds listed in Table 5 identified only one alert for the potentially reactive imino-carbonyl moieties ("*imine_one_A(321)*").

As discussed above, the reaction of the inhibitor carbonyl groups with the catalytic serine hydroxyl indeed play a important role in the proposed mechanism of action of the arylhydrazone derivatives containing TFK and ester groups. Their specific activity was confirmed by their selectivity to CES over AChE and BChE and by the structure-activity relationships identified in the experiment and explained by molecular modeling, as well as by kinetic studies, experimental concentration-response curves, and IC_{50} measurements. ABTS-scavenging activity of the compounds was confirmed by their experimentally determined structure-activity relationships, which agreed with the calculated HOMO-LUMO gaps, experimental concentration-response curves for TEAC

Table 4
Cytotoxicity of HOPs **3** and their acute toxicity in mice.

Compound 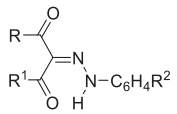				Cytotoxicity, IC_{50}, μM	Dose, mg/kg	Viability after 14 days (number of animals in the experiment/number of survivors)
No.	R	R^1	R^2			
3a	CF_3	OEt	H	>500	600	3/3
3b	CF_3	OEt	4-Me	>500	900	3/3
3c	CF_3	OEt	3-Me	>500	300	3/3
3e	CF_3	OEt	2-NO_2	>500	300	3/3
3f	CF_3	OEt	4-F	>500	n.d.	n.d.
3g	CF_3	OEt	4-Br	>500	300	3/3
3m	CF_3	OMe	2-NO_2	>500	300	3/3
3o	CHF_2	OMe	4-Me	>500	n.d.	n.d.

n.d. = not determined.

Table 5
Predicted ADMET and physicochemical profiles of HOPs **3.**

Compound				LogBB	HIA, %	hERG, pK_i	hERG, pIC_{50}	LogP_{ow}	pS	QED
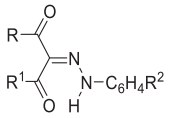										
No.	R	R^1	R^2							
3a	CF_3	OEt	H	−0.06	100	4.41	4.57	3.95	4.88	0.39
3b	CF_3	OEt	4-Me	−0.06	100	4.68	4.71	4.47	5.62	0.39
3c	CF_3	OEt	3-Me	−0.06	100	4.45	4.67	4.45	5.61	0.39
3d	CF_3	OEt	4-OMe	−0.06	100	4.68	4.66	4.12	5.32	0.38
3e	CF_3	OEt	2-NO_2	−0.41	96	3.95	4.08	3.83	4.92	0.28
3f	CF_3	OEt	4-F	−0.06	100	4.68	4.88	4.26	5.60	0.30
3g	CF_3	OEt	4-Br	−0.06	100	4.68	4.67	4.86	6.26	0.38
3h	CF_3	OEt	2-CO_2Et	−0.08	100	4.48	4.28	4.28	5.41	0.35
3i	CF_3	OEt	4-CO_2Et	−0.14	100	4.81	4.67	4.33	5.54	0.35
3j	CF_3	OMe	H	−0.06	93	4.27	4.51	3.47	4.49	0.39
3k	CF_3	OMe	4-Me	−0.06	93	4.53	4.65	4.07	5.14	0.40
3l	CF_3	OMe	4-OMe	−0.06	93	4.53	4.60	3.64	4.94	0.39
3m	CF_3	OMe	2-NO_2	−0.41	90	3.82	4.02	3.55	4.67	0.29
3n	CF_2H	OEt	4-Me	−0.06	100	4.68	4.57	3.93	4.27	0.38
3o	CF_2H	OMe	4-Me	−0.06	93	4.53	4.51	3.58	4.04	0.38
3p	C_2F_5	OEt	4-Me	−0.06	100	4.68	4.83	5.22	6.36	0.28
3q	C_3F_7	OEt	4-Me	−0.06	100	4.68	4.98	5.76	6.01	0.25
3r	C_3F_7	OMe	4-OMe	−0.06	93	4.53	4.87	5.38	5.47	0.25
3s	C_4F_9	OEt	4-Me	−0.06	100	4.68	5.09	6.17	6.59	0.21
3t	Me	OEt	4-Me	−0.06	100	4.68	4.49	2.71	3.85	0.37

Note: LogBB − blood-brain barrier permeability, HIA − human intestinal absorption [%], hERG pK_i − hERG potassium channel affinity [−log(M)], hERG pIC_{50} − hERG potassium channel inhibitory activity [−log(M)], LogP_{ow} − octanol-water partition coefficient, pS − aqueous solubility [−log(M)], QED − quantitative estimate of drug-likeness.

determination, and IC_{50} measurements. Thus, we have demonstrated in several different experimental assays and computational approaches that the compounds flagged by the PAINS screen were genuinely active.

3. Conclusions

In summary, an expanded series of HOPs **3** using the more productive synthetic protocol via $Cu(OAc)_2$-catalyzed azo coupling was obtained while 2-arylhydrazinylidene-1,3-diketones **5** were prepared from lithium 1,3-diketonates as the starting reagents. According to physical structural studies and QM calculations, 2-arylhydrazinylidene-3-oxo-3-polyfluoroalkylpropionates **3** exist as *Z*-isomers with intramolecular hydrogen bond between the NH-group and the carbonyl oxygen atom of the ester group.

All of the fully fluorinated HOPs **3**, in contrast to their CHF_2 and CH_3 derivatives and 1,3-diketone analogs **5**, were potent and highly selective inhibitors of porcine liver CES and moderate or weak inhibitors of cholinesterases. Among the studied CES inhibitors, selectivity to both human CES1 and CES2 were found, while the selectivity to CES1 was more pronounced. It should be stressed that their inhibitory concentrations are at least several orders of magnitude lower than toxic concentrations, ensuring extremely wide safety margins.

Steady-state kinetics studies showed that HOPs **3** are mixed type inhibitors of all three esterases.

To exhibit maximum anti-CES activity, a molecule based on the polyfluoroalkyl-2-imino-1,3-dione scaffold should contain a combination of a TFK group and an ester group.

Molecular docking studies demonstrated the possibility of both functional groups in the structure of HOP − TFK and ester groups − binding to the CES active site. This suggests the possibility of subsequent reactions according to two mechanisms: (1) formation of a tetrahedral adduct; and (2) a slow hydrolysis reaction. The latter could be followed by reinhibition of the enzyme by the hydrolysis product. Mechanisms of these reactions have been described using extensive QM/MM calculations (unpublished results; manuscript in preparation).

The results of molecular modeling allowed us to explain some structure-activity relationships of CES inhibition by HOPs **3,** their selectivity toward CES in comparison with cholinesterases, and the higher selectivity of pentafluoroethyl-substituted HOP **3p** to hCES1 compared to hCES2.

Computational ADMET studies revealed that all HOPs **3** were predicted to have good intestinal absorption and blood-brain barrier permeability, low cardiac toxicity risks, good lipophilicity and aqueous solubility, and reasonable overall drug-likeness, i.e. they should have good or acceptable properties for potential lead compounds at the early drug development stages.

In addition, HOPs **3**, which have a TFK group and electron-donor substituents in the arylhydrazone moiety, were found to be potent antioxidants. Accordingly, we anticipate that the radical-scavenging action of the developed selective inhibitors of CES enzymes would be an additional useful feature that could protect the liver from damage induced by highly reactive metabolites formed during the P450-mediated biotransformation of drugs. All tested compounds **3** possessed low cytotoxicity and low acute toxicity.

Thus, using kinetic studies and molecular modeling, we have shown that the high anti-CES activity of HOPs based on a polyfluoroalkyl-2-imino-1,3-dione scaffold is due to the presence of two functional groups, TFK and an ester, capable of interacting with the active site of the enzyme. Overall, the results indicate that HOPs **3** have the potential to be good candidates as human CES inhibitors for biomedicinal applications.

4. Experimental section

4.1. Chemistry

All solvents, chemicals, and reagents were obtained

commercially and used without purification. Melting points were measured in open capillaries on a Stuart SMP30 melting point apparatus and were uncorrected. The ^{1}H NMR spectra were registered on a Bruker DRX-400 (400 MHz) or Bruker Avance^{III} 500 (500 MHz) spectrometers relative to $SiMe_4$. The ^{19}F NMR spectra were obtained on a Bruker DRX-400 (376 MHz) or Bruker Avance^{III} 500 (470 MHz) spectrometers using C_6F_6 as an internal standard. The microanalyses (C, H, N) were carried out on a PerkinElmer PE 2400 series II elemental analyzer.

General Procedures for synthesis of compounds ***3.*** To 60 ml of a solution of amine (40 mmol) in 1 M hydrochloric acid, a solution of sodium nitrite (2.76 g, 40 mmol) in 40 ml of water at 0 °C was added dropwise. Then, in another container, solutions of copper (II) acetate (20 mmol) in water (20 ml) and 3-oxo ester **1** (40 mmol) in acetone (20 ml) were mixed. To the resulting suspension, a solution of the aryldiazonium salt **2** was slowly added dropwise at 10 °C. The resulting product **3** was extracted by chloroform (2 × 20 ml), and the chloroform layer was separated and dried with anhydrous sodium sulfate. The chloroform was removed *in vacuo*, and compound **3** was recrystallized from ethanol.

Ethyl (2Z)-4,4,4-trifluoro-3-oxo-2-(2-phenylhydrazinylidene)butanoate (**3a**) was obtained according to the general procedure from 3-oxo ester **1a** (7.36 g, 40 mmol) and benzenediazonium chloride prepared from aniline (3.75 g, 40 mmol) as a yellow powder (9.56 g, 83% yield), mp 90–91 °C [53,77]. ^{1}H NMR (400 MHz, DMSO-d_6): δ 1.32 (t, $^3J_{H,H}$ 7.1 Hz, 3H, OCH_2*Me*), 4.36 (q, $^3J_{H,H}$ 7.1 Hz, 2H, OCH_2Me), 7.25–7.28, 7.46–7.50, 7.56–7.58 (all m, 4H, C_6H_4), 12.95 (s, 1H, NH). ^{19}F NMR (470 MHz, DMSO-d_6): δ 93.35 (s, CF_3).

Ethyl (2Z)-4,4,4-trifluoro-2-[2-(4-methylphenyl)hydrazinylidene]-3-oxobutanoate (**3b**) was obtained according to the general procedure from 3-oxo ester **1a** (7.36 g, 40 mmol) and 4-methylbenzenediazonium chloride prepared from 4-toluidine (4.28 g, 40 mmol) as a yellow powder (13.74 g, 87% yield), mp 75–76 °C [53]. ^{1}H NMR (400 MHz, DMSO-d_6): δ 1.28 (t, $^3J_{H,H}$ 7.1 Hz, 3H, OCH_2*Me*), 2.28 (s, 3H, C_6H_4*Me*), 4.30 (q, $^3J_{H,H}$ 7.1 Hz, 2H, OCH_2Me), 7.18–7.36 (m, 4H, C_6H_4), 11.65 (s, 1H, NH). ^{19}F NMR (376 MHz, DMSO-d_6): δ 93.5 (s, CF_3).

Ethyl (2Z)-4,4,4-trifluoro-2-[2-(3-methylphenyl)hydrazinylidene]-3-oxobutanoate (**3c**) was obtained according to the general procedure from 3-oxo ester **1a** (7.36 g, 40 mmol) and 3-methylbenzenediazonium chloride prepared from *m*-toluidine (4.28 g, 40 mmol) as a yellow powder (12.95 g, 82% yield), mp 61–62 °C (eluent – $CHCl_3$). ^{1}H NMR (400 MHz, $CDCl_3$): δ 1.42 (t, $^3J_{H,H}$ 7.1 Hz, 3H, OCH_2*Me*), 2.40 (s, 3H, C_6H_4–*Me*), 4.41 (q, $^3J_{H,H}$ 7.1 Hz, 2H, OCH_2Me), 7.06–7.08, 7.23–7.24, 7.30–7.32 (all m, 4H, C_6H_4), 13.46 (s, 1H, NH). ^{19}F NMR (470 MHz, $CDCl_3$): δ 91.31 (s, CF_3). Elemental analysis calculated (%) for $C_{13}H_{13}F_3N_2O_3$ (*M* 302.25): C 51.66, H 4.34, N 9.27. Found: C 51.73, H 4.39, N 9.14.

Ethyl (2Z)-4,4,4-trifluoro-2-[2-(4-methoxyphenyl)hydrazinylidene]-3-oxobutanoate (**3d**) was obtained according to the general procedure from 3-oxo ester **1a** (7.36 g, 40 mmol) and 4-methoxybenzenediazonium chloride prepared from 4-anisidine (4.92 g, 40 mmol) as a yellow powder (13.48 g, 82% yield), mp 130–131 °C [66]. ^{1}H NMR (400 MHz, DMSO-d_6): δ 1.32 (t, $^3J_{H,H}$ 7.1 Hz, 3H, OCH_2*Me*), 3.78 (s, 3H, C_6H_4–O*Me*), 4.34 (q, $^3J_{H,H}$ 7.1 Hz, 2H, OCH_2Me), 7.06, 7.54 (both d, $^3J_{H,H}$ 9.0 Hz, 4H, C_6H_4), 13.10 (s, 1H, NH). ^{19}F NMR (376 MHz, DMSO-d_6): δ 93.52 (s, CF_3).

Ethyl (2Z)-4,4,4-trifluoro-2-[2-(2-nitrophenyl)hydrazinylidene]-3-oxobutanoate (**3e**) was obtained according to the general procedure from 3-oxo ester **1a** (7.36 g, 40 mmol) and 2-nitrobenzenediazonium chloride prepared from 2-nitroaniline (5.52 g, 40 mmol) as a yellow powder (10.78 g, 81% yield), mp 99–100 °C [53]. ^{1}H NMR (400 MHz, $CDCl_3$): δ 1.45 (t, $^3J_{H,H}$ 7.1 Hz, 3H, OCH_2*Me*), 4.5 (q, $^3J_{H,H}$ 7.1 Hz, 2H, OCH_2Me), 7.34, 7.73, 8.07, 8.30 (all m, 4H, C_6H_4), 14.71 (s, 1H, NH). ^{19}F NMR (376 MHz, $CDCl_3$): δ 90.96 (s, CF_3). Elemental analysis calculated (%) for $C_{12}H_{10}F_3N_3O_5$ (*M* 333.06): C 43.25, H 3.02, F 17.10, N 12.61. Found: C 43.15, H 3.07, F 17.35, N 12.80.

Ethyl (2Z)-4,4,4-trifluoro-2-[2-(4-fluorophenyl)hydrazinylidene]-3-oxobutanoate (**3f**) was obtained according to the general procedure from 3-oxo ester **1a** (7.36 g, 40 mmol) and 4-fluorobenzenediazonium chloride prepared from 4-fluoroaniline (4.44 g, 40 mmol) as an orange powder (10.02 g, 82% yield), mp 79–80 °C (eluent – CH_2Cl_2). ^{1}H NMR (400 MHz, $CDCl_3$): δ 1.42 (t, $^3J_{H,H}$ 7.1 Hz, 3H, OCH_2*Me*), 4.41 (q, $^3J_{H,H}$ 7.1 Hz, 2H, OCH_2Me), 7.12–7.17, 7.38–7.42 (both m, 4H, C_6H_4), 13.52 (s, 1H, NH). ^{19}F NMR (376 MHz, $CDCl_3$): δ 47.08 (m, 1F, F_{Ar}), 91.28 (s, 3F, CF_3). Elemental analysis calculated (%) for $C_{12}H_{10}F_4N_2O_3$ (*M* 306.22): C 47.07, H 3.29, N 9.15. Found: C 47.06, H 3.03, N 9.33.

Ethyl (2Z)-4,4,4-trifluoro-2-[2-(4-bromophenyl)hydrazinylidene]-3-oxobutanoate (**3g**) was obtained according to the general procedure from 3-oxo ester **1a** (7.36 g, 40 mmol) and 4-bromobenzenediazonium chloride prepared from 4-bromoaniline (6.88 g, 40 mmol) as a yellow powder (11.75 g, 80% yield), mp 109–110 °C (eluent – CH_2Cl_2). ^{1}H NMR (400 MHz, $CDCl_3$): δ 1.42 (t, $^3J_{H,H}$ 7.1 Hz, 3H, OCH_2*Me*), 4.41 (q, $^3J_{H,H}$ 7.1 Hz, 2H, OCH_2Me), 7.29, 7.56 (both d, $^3J_{H,H}$ 8.8 Hz, 4H, C_6H_4), 13.44 (s, 1H, NH). ^{19}F NMR (376 MHz, $CDCl_3$): δ 91.19 (s, CF_3). Elemental analysis calculated (%) for $C_{12}H_{10}BrF_3N_2O_3$ (*M* 367.12): C 39.26, H 2.75, N 7.63. Found: C 39.35, H 2.72, N 7.41.

Ethyl 2-[(2Z)-2-(1-ethoxy-4,4,4-trifluoro-1,3-dioxobutan-2-ylidene) hydrazinyl]benzoate (**3h**) was obtained according to the general procedure from 3-oxo ester **1a** (7.36 g, 40 mmol) and 2-(ethoxycarbonyl) benzenediazonium chloride prepared from 2-ethoxycarbonylaniline (6.60 g, 40 mmol) as a yellow powder (12.38 g, 86% yield), mp 104–105 °C (EtOH). ^{1}H NMR (500 MHz, $CDCl_3$): δ 1.44 (m, 6H, $2OCH_2$*Me*), 4.49 (m, 4H, $2OCH_2$Me), 7.24–7.27, 7.63–7.66, 7.96–7.97, 8.09–8.11 (all m, 4H, C_6H_4), 14.88 (s, 1H, NH). ^{19}F NMR (470 MHz, $CDCl_3$): δ 91.31 (s, CF_3).

^{1}H NMR (500 MHz, DMSO-d_6): δ 1.36 (m, 6H, $2OCH_2$*Me*), 4.40 (m, 4H, $2OCH_2$Me), 7.35–7.39, 7.80–7.83, 8.05–8.07 (all m, 4H, C_6H_4), 14.59 (s, 1H, NH). ^{19}F NMR (470 MHz, DMSO-d_6): δ 93.19 (s, CF_3). Elemental analysis calculated (%) for $C_{15}H_{15}F_3N_2O_5$ (*M* 360.29): C 50.01, H 4.20, N 7.78. Found: C 50.04, H 4.07, N 7.74.

Ethyl 4-[(2Z)-2-(1-ethoxy-4,4,4-trifluoro-1,3-dioxobutan-2-ylidene) hydrazinyl]benzoate (**3i**) was obtained according to the general procedure from 3-oxo ester **1a** (7.36 g, 40 mmol) and 4-(ethoxycarbonyl) benzenediazonium chloride prepared from 4-ethoxycarbonylaniline (6.60 g, 40 mmol) as a yellow powder (11.81 g, 82% yield), mp 106–107 °C (EtOH). ^{1}H NMR (500 MHz, $CDCl_3$): δ 1.41, 1.43 (both t, $^3J_{H,H}$ 7.1 Hz, 6H, $2OCH_2$*Me*), 4.39, 4.43 (both q, $^3J_{H,H}$ 7.1 Hz, 4H, $2OCH_2$Me), 7.45, 8.13 (both d, $^3J_{H,H}$ 8.8 Hz, 4H, C_6H_4), 13.43 (s, 1H, NH). ^{19}F NMR (470 MHz, $CDCl_3$): δ 91.09 (s, CF_3). Elemental analysis calculated (%) for $C_{15}H_{15}F_3N_2O_5$ (*M* 360.29): C 50.01, H 4.20, N 7.78. Found: C 50.12, H 4.21, N 7.60.

Methyl (2Z)-4,4,4-trifluoro-3-oxo-2-(2-phenylhydrazinylidene)butanoate (**3j**) was obtained according to the general procedure from 3-oxo ester **1b** (7.36 g, 40 mmol) and benzenediazonium chloride prepared from aniline (3.75 g, 40 mmol) as orange crystals (8.76 g, 80% yield), mp 84–85 °C (MeOH). ^{1}H NMR (400 MHz, $CDCl_3$): δ 3.96 (s, 3H, OMe), 7.27–7.29, 7.44–7.45 (both m, 5H, Ph), 13.49 (s, 1H, NH). ^{19}F NMR (376 MHz, $CDCl_3$): δ 91.31 (d, *J* 0.7 Hz, CF_3). Elemental analysis calculated (%) for $C_{11}H_9F_3N_2O_3$ (*M* 274.20): C 48.18, H 3.31, N 10.22. Found: C 48.24, H 3.15, N 10.20.

Methyl (2Z)-4,4,4-trifluoro-2-[2-(4-methylphenyl)hydrazinylidene]-3-oxobutanoate (**3k**) was obtained according to the general procedure

from 3-oxo ester **1b** (7.36 g, 40 mmol) and 4-methylbenzene diazonium chloride prepared from 4-toluidine (4.28 g, 40 mmol) as orange crystals (9.91 g, 86% yield), mp 111–112 °C (eluent – $CHCl_3$). ^{1}H NMR (500 MHz, $CDCl_3$): δ 2.38 (s, 3H, C_6H_4–*Me*), 3.94 (s, 3H, OMe), 7.24, 7.33 (both d, $^3J_{H,H}$ 8.4 Hz, 4H, C_6H_4), 13.52 (s, 1H, NH). ^{19}F NMR (470 MHz, $CDCl_3$): δ 91.37 (s, CF_3). Elemental analysis calculated (%) for $C_{12}H_{11}F_3N_2O_3$ (*M* 288.23): C 50.01, H 3.85, N 9.72. Found: C 49.85, H 3.77, N 9.66.

Methyl (2Z)-4,4,4-trifluoro-2-[2-(4-methoxyphenyl)hydrazinylidene]-3-oxobutanoate (**3l**) was obtained according to the general procedure from 3-oxo ester **1b** (7.36 g, 40 mmol) and 4-methoxybenzenediazonium chloride prepared from 4-anisidine (4.92 g, 40 mmol) as an orange powder (10.58 g, 87% yield), mp 142–144 °C [66].

Methyl (2Z)-4,4,4-trifluoro-2-[2-(2-nitrophenyl)hydrazinylidene]-3-oxobutanoate (**3m**) was obtained according to the general procedure from 3-oxo ester **1b** (7.36 g, 40 mmol) and 2-nitrobenzenediazonium chloride prepared from 2-nitroaniline (5.52 g, 40 mmol) as an orange powder (10.59 g, 83% yield), mp 123–124 °C (MeOH). ^{1}H NMR (500 MHz, $CDCl_3$): δ 4.02 (s, 3H, OMe), 7.33–7.37, 7.76–7.79, 8.06–8.08, 8.30–8.32 (all m, 4H, C_6H_4), 14.77 (s, 1H, NH). ^{19}F NMR (470 MHz, $CDCl_3$): δ 90.99 (d, *J* 0.6 Hz, CF_3). Elemental analysis calculated (%) for $C_{11}H_8F_3N_3O_5$ (*M* 319.20): C 41.39, H 2.53, N 13.16. Found: C 41.43, H 2.64, N 13.19.

Ethyl (2Z)-4,4-difluoro-2-[2-(4-methylphenyl)hydrazinylidene]-3-oxobutanoate (**3n**) was obtained according to the general procedure from 3-oxo ester **1c** (6.64 g, 40 mmol) and 4-methylbenzenediazonium chloride prepared from 4-toluidine (4.28 g, 40 mmol) as yellow crystals (9.42 g, 83% yield), mp 96–97 °C [67]. ^{1}H NMR (500 MHz, DMSO-d_6): 1.31 (t, $^3J_{H,H}$ 7.1 Hz, 3H, OCH_2*Me*), 2.31 (s, 3H, C_6H_4–*Me*), 4.34 (q, $^3J_{H,H}$ 7.1 Hz, 2H, OCH_2), 7.05 (t, $^2J_{H,F}$ 53.7 Hz, 1H, HCF_2), 7.24–7.26, 7.48–7.50 (all m 4H, C_6H_4), 12.71 (s, 1H, NH). ^{19}F NMR (470 MHz, DMSO-d_6): δ 35.25 (d, $^2J_{H,F}$ 53.7 Hz, HCF_2).

Methyl (2Z)-4,4-difluoro-2-[2-(4-methylphenyl)hydrazinylidene]-3-oxobutanoate (**3o**) was obtained according to the general procedure from 3-oxo ester **1d** (6.08 g, 40 mmol) and 4-methylbenzenediazonium chloride prepared from 4-toluidine (4.28 g, 40 mmol) as an orange powder (8.64 g, 80% yield), mp 102–103 °C [67]. ^{1}H, ^{19}F NMR (DMSO-d_6) described in Ref. [67].

Ethyl (2Z)-4,4,5,5,5-pentafluoro-2-[2-(4-methylphenyl)hydrazinylidene]-3-oxopentanoate (**3p**) was obtained according to the general procedure from 3-oxo ester **1e** (9.36 g, 40 mmol) and 4-methylbenzenediazonium chloride prepared from 4-toluidine (4.28 g, 40 mmol) as a yellow powder (11.97 g, 85% yield), mp 53–54 °C (eluent – $CHCl_3$). ^{1}H NMR (400 MHz, $CDCl_3$): δ 1.42 (t, $^3J_{H,H}$ 7.1 Hz, 3H, OCH_2*Me*), 2.38 (s, 3H, C_6H_4–*Me*), 4.40 (q, $^3J_{H,H}$ 7.1 Hz, 2H, OCH_2Me), 7.24, 7.32 (both d, $^3J_{H,H}$ 8.4 Hz, 4H, C_6H_4), 13.56 (s, 1H, NH). ^{19}F NMR (376 MHz, $CDCl_3$): δ 47.08 (m, 2F, CF_2), 80.76 (m, 3F, CF_3). ^{1}H NMR (400 MHz, DMSO-d_6): δ 1.32 (t, $^3J_{H,H}$ 7.1 Hz, 3H, OCH_2*Me*), 2.32 (s, 3H, C_6H_4–*Me*), 4.34 (q, $^3J_{H,H}$ 7.1 Hz, 2H, OCH_2Me), 7.29, 7.45 (both d, $^3J_{H,H}$ 8.4 Hz, 4H, C_6H_4), 12.96 (s, 1H, NH). ^{19}F NMR (376 MHz, DMSO-d_6): δ 48.49 (m, 2F, CF_2), 82.14 (m, 3F, CF_3). Elemental analysis calculated (%) for $C_{14}H_{13}F_5N_2O_3$ (*M* 352.26): C 47.74, H 3.72, N 7.95. Found: C 47.83, H 3.65, N 8.01.

Ethyl (2Z)-4,4,5,5,6,6,6-heptafluoro-2-[2-(4-methylphenyl)hydrazinylidene]-3- oxohexanoate (**3q**) was obtained according to the general procedure from 3-oxo ester **1f** (11.36 g, 40 mmol) and 4-methylbenzenediazonium chloride prepared from 4-toluidine (4.28 g, 40 mmol) as a yellow powder (13.98 g, 87% yield), mp 38–39 °C. (eluent – $CHCl_3$). ^{1}H NMR (400 MHz, $CDCl_3$): δ 1.42 (t, $^3J_{H,H}$ 7.1 Hz, 3H, OCH_2*Me*), 2.37 (s, 3H, C_6H_4–*Me*), 4.40 (q, $^3J_{H,H}$ 7.1 Hz, 2H, OCH_2Me), 7.24, 7.30 (both d, $^3J_{H,H}$ 8.4 Hz, 4H, C_6H_4), 13.56 (s, 1H, NH). ^{19}F NMR (376 MHz, $CDCl_3$): δ 37.49 (m, 2F, CF_2), 49.51 (m, 2F, CF_2), 81.37 (m, 3F, CF_3). ^{1}H NMR (400 MHz, DMSO-d_6): δ), 3.78, 3.85 (both s, 6H, C_6H_4–O*Me*, O*Me*), 7.06, 7.51 (both d, $^3J_{H,H}$ 8.4 Hz, 4H, C_6H_4), 13.03 (s, 1H, NH). ^{19}F NMR (376 MHz, DMSO-d_6): δ 38.48 (m, 2F, CF_2), 50.99 (m, 2F, CF_2), 82.81 (m, 3F, CF_3). Elemental analysis calculated (%) for $C_{15}H_{13}F_7N_2O_3$ (*M* 402.27): C 44.79, H 3.26, N 6.96. Found: C 44.69, H 3.15, N 6.78.

Methyl (2Z)-4,4,5,5,6,6,6-heptafluoro-2-[2-(4-methoxyphenyl) hydrazinylidene]-3-oxohexanoate (**3r**) was obtained according to the general procedure from ester **1g** (10.80 g, 40 mmol) and 4-methoxybenzenediazonium chloride prepared from 4-anisidine (4.92 g, 40 mmol) as a yellow powder (13.25 g, 82% yield), mp 95–96 °C [67] ^{1}H NMR (500 MHz, DMSO-d_6): 1.31 (t, $^3J_{H,H}$ 7.1 Hz, 3H, OCH_2*Me*), 2.31 (s, 3H, C_6H_4–*Me*), 4.34 (q, $^3J_{H,H}$ 7.1 Hz 2H, OCH_2), 7.05 (t, $^2J_{H,F}$ 53.7 Hz, 1H, HCF_2), 7.24–7.26, 7.48–7.50 (all m 4H, C_6H_4), 12.71 (s, 1H, NH). ^{19}F NMR (470 MHz, DMSO-d_6): δ 35.25 (d, $^2J_{H,F}$ 53.7 Hz, HCF_2).

Ethyl (2Z)-4,4,5,5,6,6,7,7,7-nonafluoro-2-[2-(4-methylphenyl)hydrazinylidene]-3-oxoheptanoate (**3s**) was obtained according to the general procedure from ester **1h** (13.36 g, 40 mmol) and 4-methylbenzenediazonium chloride prepared from 4-toluidine (4.28 g, 40 mmol) as a yellow powder (14.30 g, 82% yield), mp 43–45 °C [78]. ^{1}H NMR (400 MHz, DMSO-d_6): δ 1.31 (t, $^3J_{H,H}$ 7.1 Hz, 3H, OCH_2*Me*), 2.31 (s, 3H, C_6H_4–*Me*), 4.35 (q, $^3J_{H,H}$ 7.1 Hz, 2H, OCH_2Me), 7.28, 7.44 (both d, $^3J_{H,H}$ 8.4 Hz, 4H, C_6H_4), 12.92 (s, 1H, NH). ^{19}F NMR (376 MHz, DMSO-d_6): δ 37.66 (m, 2F, CF_2), 41.88 (m, 2F, CF_2), 51.33 (m, 2F, CF_2), 82.20 (m, 3F, CF_3).

Ethyl (2E)-2-[2-(4-methylphenyl)hydrazinylidene]-3-oxobutanoate (**3t**) was obtained according to the general procedure from ester **1i** (5.20 g, 40 mmol) and 4-methylbenzenediazonium chloride prepared from 4-toluidine (4.28 g, 40 mmol) as an orange powder (8.13 g, 82% yield), mp 80–81 °C [77]. ^{1}H NMR (400 MHz, DMSO-d_6): *Z*-isomer (70%): δ 1.29 (t, $^3J_{H,H}$ 7.1 Hz, 3H, OCH_2*Me*), 2.28 (s, 3H, C_6H_4–*Me*), 2.37 (s, 3H, Me), 4.30 (q, $^3J_{H,H}$ 7.1 Hz, 2H, OCH_2Me), 7.19, 7.34 (both d, $^3J_{H,H}$ 8.4 Hz, 4H, C_6H_4), 11.65 (s, 1H, NH), *E*-isomer (70%): δ1.29 (t, $^3J_{H,H}$ 7.1 Hz, 3H, OCH_2*Me*), 2.30 (s, 3H, C_6H_4–*Me*), 2.37 (s, 3H, Me), 4.25 (q, $^3J_{H,H}$ 7.1 Hz, 2H, OCH_2Me), 7.23, 7.41 (both d, $^3J_{H,H}$ 8.4 Hz, 4H, C_6H_4), 14.37 (s, 1H, NH).

General Procedures for synthesis of compounds ***5.*** To a solution of amine (40 mmol) in a solution of 1 M hydrochloric acid (60 ml) was added dropwise a solution of sodium nitrite (2.76 g, 40 mmol) in 40 ml of water at 0 °C. Then, in another container, solutions of sodium acetate (40 mmol) in water (20 ml) and lithium salt **4** (40 mmol) in ethanol (20 ml) were mixed. To the resulting suspension was slowly dripped solution of the aryldiazonium salt **2** at 10 °C. The resulting product **5** was extracted by chloroform (2 × 20 ml), dried with sodium sulfate. The chloroform was removed in vacuum. The compound **5** was recrystallized from ethanol.

(3E)-1,1,1-Trifluoro-3-[2-(4-methylphenyl)hydrazinylidene] pentane-2,4-dione (**5a**) was obtained according to the general procedure from lithium salt **4a** (6.40 g, 40 mmol) and 4-methylben zenediazonium chloride prepared from 4-toluidine (4.28 g, 40 mmol) as a yellow powder (8.70 g, 80% yield), mp 95–96 °C. ^{1}H NMR (400 MHz, $CDCl_3$): δ 2.38 (s, 3H, C_6H_4–*Me*), 2.63 (s, 3H, *Me*), 7.25, 7.38 (both d, $^3J_{H,H}$ 8.5 Hz, 4H, C_6H_4), 15.25 (s, 1H, NH). ^{19}F NMR (376 MHz, $CDCl_3$): δ 91.60 (s, 3F, CF_3). ^{1}H NMR (400 MHz, DMSO-d_6): δ 2.33 (s, 3H, C_6H_4–*Me*), 2.53 (s, 3H, *Me*), 7.31, 7.54 (both d, $^3J_{H,H}$ 8.5 Hz, 4H, C_6H_4), 14.66 (s, 1H, NH). ^{19}F NMR (376 MHz, DMSO-d_6): δ 93.70 (s, CF_3). Elemental analysis calculated (%) for $C_{12}H_{11}F_3N_2O_2$ (*M* 272.23): C 52.95, H 4.07, N 10.29. Found: C 52.74, H 4.17, N 10.22.

(2E)-4,4,4-Trifluoro-2-[2-(4-methylphenyl)hydrazinylidene]-1-phenylbutane-1,3-dione (**5b)** was obtained according to the general procedure from lithium salt **4b** (8.88 g, 40 mmol) and 4-methylbenzenediazonium chloride prepared from 4-toluidine (4.28 g, 40 mmol) as a yellow powder (8.70 g, 80% yield), mp 133–134 °C [79] ^{1}H NMR (400 MHz, DMSO-d_6): δ 2.30 (s, 3H,

C_6H_4–*Me*), 7.24–7.26, 7.37–7.40, 7.56–7.60, 7.70–7.74, 7.80–7.82 (all m, 9H, C_6H_4, C_6H_5), 12.52 (s, 1H, NH). ^{19}F NMR (376 MHz, DMSO-d_6): δ 93.49 (s, CF_3).

4.2. Inhibition in vitro of porcine liver CES, human CES1 and CES2, human AChE, and equine BChE

The following enzymes were purchased from Sigma-Aldrich (Saint Louis, MO, USA): porcine liver carboxylesterase (CES, EC 3.1.1.1), human recombinant carboxylesterases CES1 (E0287, Carboxylesterase 1 isoform b human recombinant, expressed in baculovirus-infected BTI insect cells) and CES2 (E4749, Carboxylesterase 2 human recombinant, expressed in mouse NSO cells, ≥95% (SDS-PAGE)), human erythrocyte acetylcholinesterase (AChE, EC 3.1.1.7) and equine serum butyrylcholinesterase (BChE, EC 3.1.1.8).

Substrates for CES, AChE, and BChE were 4-nitrophenyl acetate (4-NPA), acetylthiocholine iodide (ATCh), and butyrylthiocholine iodide (BTCh), respectively, and the colorimetric reagent for the AChE and BChE assays was 5,5′-dithio-bis-(2-nitrobenzoic acid) (DTNB) (Sigma-Aldrich).

All the kinetic experiments were performed under standard conditions, according to the protocol of IPAC RAS for a reversible inhibitors study.

CES (porcine liver) activity was assessed colorimetrically in 0.1 M K/Na phosphate buffer pH 8.0, 25 °C, by measuring the absorbance of 4-nitrophenol at 405 nm [80]. Final enzyme and substrate (4-NPA) concentrations were 0.02 unit/mL and 1 mM, respectively. Reagent blanks included all constituents except enzyme.

The activity of hCES1 and hCES2 were determined spectrophotometrically by the release of 4-nitrophenol at 405 nm [80]. The assay solution consisted of 0.1 M K/Na phosphate buffer pH 7.4, 25 °C as well as 1 mM 4-nitrophenyl acetate and 0.02 unit/mL of hCES1 or 0.01 unit/mL of hCES2. Assays were carried out with a blank containing all components except CES1 and CES2, respectively.

Ellman's colorimetric assay was used to measure AChE and BChE activity in 0.1 M K/Na phosphate buffer at pH 7.5, 25 °C [81]. Final concentrations of reactants were 0.33 mM DTNB, 0.02 unit/mL of AChE or BChE and 1 mM of substrate (ATCh or BTCh, respectively). Reagent blanks consisted of reaction mixtures without enzyme to assess non-enzymatic hydrolysis of substrates.

Test compounds were dissolved in DMSO. Reaction mixtures contained a final DMSO concentration of 2% (v/v). This concentration of DMSO on its own did not significantly affect the activity of any of the enzymes in the study (data not shown). Enzyme inhibition was first assessed at a single concentration of 20 μM for each compound after a 10 min incubation at 25 °C in three separate experiments. The most active compounds were then selected for determination of the IC_{50} (inhibitor concentration resulting in 50% inhibition of control enzyme activity). Compounds (eight concentrations ranging between 10^{-12} and 10^{-4} M were selected to achieve 20–80% inhibition) were incubated with each enzyme for 10 min at 25 °C. Substrate was then added and residual enzyme activity relative to an inhibitor-free control was measured using a FLUOStar Optima microplate reader (LabTech, Ortenberg, Germany).

4.3. Porcine liver CES, human AChE, and equine BChE inhibition kinetics: inhibition constants at steady state

To elucidate the inhibition mechanisms for active compounds, porcine liver CES, human erythrocyte AChE, and equine serum BChE residual activities were determined in the presence of 3 increasing concentrations of a test compound and 5–6 decreasing concentrations of the substrates. Test compounds were incubated with the enzymes at 25 °C for 10 min, followed by the addition of substrates. A parallel control was made to assay of the rate of hydrolysis of the same concentrations of substrates in solutions with no inhibitor. Kinetic parameters of substrate hydrolysis were determined. Measurements were performed in a FLUOStar Optima microplate reader (LabTech, Ortenberg, Germany). Each experiment was performed in triplicate.

4.4. ABTS radical cation scavenging assay

The antioxidant activity of compounds **3** and **5** was evaluated by the ABTS radical cation ($ABTS^{\bullet+}$) scavenging assay by the ability of the compounds to decolorize the $ABTS^{\bullet+}$ solution [76] with some modifications [56,58]. Trolox was used as the antioxidant standard, and the well-known antioxidants ascorbic acid and catechol were used as the comparison compounds. All tested compounds and standards were dissolved in DMSO.

ABTS (2,2′-azinobis-(3-ethylbenzothiazoline-6-sulfonic acid)) was purchased from Tokyo Chemical Industry Co. Ltd. (Tokyo, Japan). Potassium persulfate (di-potassium peroxydisulfate), Trolox® (6-hydroxy-2,5,7,8-tetramethylchroman-2-carboxylic acid), ascorbic acid, catechol, and HPLC-grade ethanol were obtained from Sigma-Aldrich Chemical Co. Aqueous solutions were prepared using deionized water.

The solution of $ABTS^{\bullet+}$ was produced by incubation of ABTS with potassium persulfate in deionized water for 12–16 h at room temperature in the dark. Radical scavenging capacity of the compounds was analyzed by mixing 10 μl of compound with 240 μl of $ABTS^{\bullet+}$ working solution in ethanol (100 μM final concentration), and after 1 h of incubation the decrease in absorbance was measured spectrophotometrically at 734 nm using a Bio-Rad xMark microplate UV/VIS spectrophotometer (Bio-Rad, Hercules, CA, USA). Ethanol blanks were run in each assay. Values were obtained from three replicates of each sample and three independent experiments.

Antioxidant activity was reported as Trolox equivalent antioxidant capacity (TEAC values), consisting of the ratio between the slopes obtained from the linear correlation for concentrations of the tested compounds and Trolox with absorbance of ABTS radical. For the most active compounds, we also determined IC_{50} values (compound concentration required for 50% reduction of the ABTS radical).

4.5. Cytotoxicity studies

Human fetal mesenchymal stem cells (FetMSC), non-immortalized fibroblast-like cells obtained from bone marrow of 5- to 6-week-old fetuses [82], were maintained in F12/DMEM medium supplemented with 10% (v/v) FBS, L-glutamine (3 mM), 50 IU/ml penicillin and 50 μg/ml streptomycin. The FetMSC cell line is a certified culture available from the Russian collection of vertebrate cell cultures (RCVCC) of the Institute of Cytology, Russian Academy of Sciences. The cell line was purchased from RCVCC in 2014. Mycoplasma contamination was tested quarterly with DAPI staining. A cell-line authentication procedure was not set; hence, cells were not used for more than 10–15 passages.

To investigate the cytotoxicity of compounds in FetMSC cells, the MTT cell viability assay was used [83]. Cells were plated in 96-well plates (6×10^3 cells/well). At 24 h after plating, the incubation medium was replaced with fresh medium containing test compounds at concentrations of 100, 250 and 500 μM. Control cells were treated with 0.1% (v/v) DMSO. After 72 h exposure, 0.5 mg/ml of MTT was added to each well and cells were incubated for 4 h,

then culture medium was aspirated and MTT formazan was dissolved in 100% DMSO. MTT staining intensity was read at 570 nm. The MTT staining of control cells was taken as 100%.

4.6. Acute toxicity evaluation

The toxicity evaluation was performed on CD-1 mice. Laboratory animals (CD-mice) were obtained from the Animal Unit "Pushino" at the M.M. Shemyakin and Yu. A. Ovchinnikov Institute of Bioorganic Chemistry RAS (Russia). Animals were housed in a controlled environment with a natural light cycle in polypropylene cages (Bioskape), on standard bedding (Rehofix MK 2000, J. Rettenmaier & Söhne, Germany), supplied with feed for conventional laboratory rodents (Chara, "Assortiment-Agro", Russia) and water *ad libitum*. Animal care and all the procedures were performed by professional staff according to the Federal Law N☺61-FZ [84] and guidelines for pre-clinical study of medicinal products [85]. The procedure for toxicity evaluation was based on OECD recommendations [86] and guidelines for pre-clinical study of medicinal products [85]. For general estimation of the toxicity range of synthesized compounds, three animals per group (one dose) were used for several compounds. The tested compounds in 2% (w/v) starch mucilage solution were injected intraperitoneally. Animals were observed during 14 days, the number of deaths was counted, and percent viability calculated.

4.7. Molecular modeling studies

4.7.1. Quantum mechanical calculations

Quantum mechanical optimizations of geometries of all considered compounds (*Z*-, *E*-isomers and major conformers) were performed with the GAMESS US [87] package at B3LYP/6-31G* and B3LYP/6−311++G** (for frontier orbitals calculations) levels of theory using an implicit PCM solvent model.

4.7.2. Molecular docking

An X-ray crystal structure of human CES was used for molecular modeling studies due to its high quality. Previous studies showed that the available X-ray crystal structure of the porcine enzyme had certain problems impairing its use for molecular modeling [56], while results with the homology model of the porcine enzyme were very close to those obtained with the X-ray crystal structure of the human protein.

The protein structure of hCES1 for molecular docking was prepared using the A-chain of the X-ray crystal structure PDB ID 2H7C [88] (hCES; 2.00 Å resolution); the missing Glu99 side chain was reconstructed manually. The homology model of hCES2 was prepared as described previously [56]. For cholinesterases, X-ray crystal structures of human AChE (PDB ID 4EY4 and 4EY7 [89]) and human BChE (PDB ID 1P0I [90]) were used. The BChE structure was prepared as described previously [91]. For the other two structures, all crystallographic waters and co-crystallized molecules were removed. Hydrogen atoms were added with Reduce [92] software, which protonates histidine rings with regard to the surrounding hydrogen-bonding network. The MD-optimized homology model of CES2 was described recently [56].

Partial atomic charges on ligand atoms were assigned from QM data according to the Löwdin [93] scheme, corresponding to a recent comparison of different atomic charge distribution schemes [94].

Molecular docking was performed with AutoDock 4.2.6 software [71]. The grid box for docking included the entire active site gorge of CES and AChE (22.5 Å × 22.5 Å × 22.5 Å grid box dimensions), and BChE (15 Å × 20.25 Å × 18 Å) with a grid spacing of 0.375 Å. The main Lamarckian Genetic Algorithm (LGA) [95] parameters were 256 runs, 25×10^6 evaluations, 27×10^4 generations, and a population size of 3000.

Figures for molecular structures were prepared with PyMOL (www.pymol.org).

4.8. Prediction of ADMET and physicochemical profiles

Human intestinal absorption (HIA) [96], blood-brain barrier permeability (LogBB) [97], and hERG-mediated cardiac toxicity risk (channel affinity p*Ki* and inhibitory activity pIC_{50}) [98] were estimated using the integrated online service for ADMET properties prediction ADMET Prediction Service [99] (http://qsar.chem.msu.ru/admet/Accessed Dec 01, 2020). It implements the predictive QSAR models based on accurate and representative training sets, fragmental descriptors, and artificial neural networks. The lipophilicity ($LogP_{ow}$) and aqueous solubility (pS) were estimated by the ALogPS 3.0 neural network model implemented in the OCHEM platform [100]. The quantitative estimate of drug-likeness (QED) values [101] were calculated by RDKit version 2020.03.4 software [102].

4.9. PAINS analysis

The Pan Assay INterference compoundS (PAINS) alerts were checked using RDKit version 2020.03.4 software [102]. A description of the experimental evidence for specific activity of the reported compounds with potential PAINS liability is presented in the following Results and Experimental sections: inhibition *in vitro* of porcine liver CES, human CES1 and CES2, human AChE, and equine BChE; porcine liver CES, human AChE and equine BChE inhibition kinetics: inhibition constants at steady state; and ABTS radical cation scavenging assay as a measure of antioxidant activity. Computational evidence is presented in the sections describing results and methods of quantum mechanical calculations and molecular docking.

4.10. Statistical analyses

Results are presented as mean ± SEM ($n \geq 3$ independent experiments) calculated using GraphPad Prism version 6.05 for Windows, GraphPad Software (La Jolla, CA, USA). Plots, linear regressions, and values of IC_{50}, rate, and equilibrium constants were determined using Origin 6.1 for Windows, OriginLab (Northampton, MA, USA).

Declaration of competing interest

The authors declare that they have no known competing financial interests or personal relationships that could have appeared to influence the work reported in this paper.

Acknowledgments

This work was supported by RFBR (project 20-03-00312) (synthesis and characterization of compounds) and the IPAC RAS State Targets Project No. 0090-2019-0005 (biochemical studies). Analytical studies were carried out using equipment of the Center for Joint Use "Spectroscopy and Analysis of Organic Compounds" at the Postovsky Institute of Organic Synthesis of UB RAS; biochemical studies were carried out using equipment of the "Center for Collective Use of IPAC RAS". The authors thank Dr. O.P. Krasnykh (Perm National Research Polytechnic University, Russia) for determination of acute toxicity. Computer modeling was carried out using equipment from the shared research facilities of the HPC computing resources at Lomonosov Moscow State University [103].

We thank acknowledge also the Joint Supercomputer Center of the Russian Academy of Sciences for provision of computational time. Support for RJR's contributions was provided in part by a research grant from the Alternatives Research and Development Foundation (ARDF) and an Mcubed grant from the University of Michigan. The funding sources had no role in the study design; collection, analysis and interpretation of data; writing of the manuscript; or the decision to submit the article for publication.

Appendix A. Supplementary data

Supplementary data to this article can be found online at https://doi.org/10.1016/j.ejmech.2021.113385.

Abbreviations

CES	mammalian carboxylesterase
hCES1	human carboxylesterase 1
hCES2	human carboxylesterase 2
AChE	acetylcholinesterase
BChE	butyrylcholinesterase
TFK	trifluoromethyl ketone
TEAC	Trolox equivalent antioxidant capacity
ROS	radical oxygen species
RNS	radical nitrogen species
4-NPA	4-nitrophenyl acetate
ATCh	acetylthiocholine iodide
BTCh	butyrylthiocholine iodide
DTNB	5,5′-dithio-bis-(2-nitrobenzoic acid)
DMSO	Dimethyl Sulfoxide
ADMET	absorption, distribution, metabolism, excretion, toxicity
CNS	central nervous system
LogBB	blood-brain barrier permeability
HIA	human intestinal absorption [%]
hERG *pKi*	hERG potassium channel affinity [−log(M)]
hERG pIC_{50}	hERG potassium channel inhibitory activity [−log(M)]
$LogP_{ow}$	octanol-water partition coefficient
pS	aqueous solubility [−log(M)]
QED	quantitative estimate of drug-likeness
ABTS	2,2′-azinobis-(3-ethylbenzothiazoline-6-sulfonic acid)
Trolox	6-hydroxy-2.5,7,8-tetramethylchroman-2-carboxylic acid
QM/MM	quantum mechanics/molecular mechanics
MTT	3-(4,5-dimethylthiazol-2-yl)-2,5-diphenyltetrazolium bromide;
FetMSC cells	human fetal mesenchymal stem cells

References

[1] T. Satoh, M. Hosokawa, The mammalian carboxylesterases: from molecules to functions, Annu. Rev. Pharmacol. Toxicol. 38 (1998) 257–288, https://doi.org/10.1146/annurev.pharmtox.38.1.257.

[2] P. Potter, R. Wadkins, Carboxylesterases – detoxifying enzymes and targets for drug therapy, Curr. Med. Chem. 13 (2006) 1045–1054, https://doi.org/10.2174/092986706776360969.

[3] M.J. Hatfield, R.A. Umans, J.L. Hyatt, C.C. Edwards, M. Wierdl, L. Tsurkan, M.R. Taylor, P.M. Potter, Carboxylesterases: general detoxifying enzymes, Chem. Biol. Interact. 259 (2016) 327–331, https://doi.org/10.1016/j.cbi.2016.02.011.

[4] T. Satoh, M. Hosokawa, Structure, function and regulation of carboxylesterases, Chem. Biol. Interact. 162 (2006) 195–211, https://doi.org/10.1016/j.cbi.2006.07.001.

[5] T. Imai, Human carboxylesterase isozymes: catalytic properties and rational drug design, Drug Metabol. Pharmacokinet. 21 (2006) 173–185, https://doi.org/10.2133/dmpk.21.173.

[6] M. Hosokawa, Structure and catalytic properties of carboxylesterase isozymes involved in metabolic activation of prodrugs, Molecules 13 (2008) 412–431, https://doi.org/10.3390/molecules13020412.

[7] D. Wang, L. Zou, Q. Jin, J. Hou, G. Ge, L. Yang, Human carboxylesterases: a comprehensive review, Acta Pharm. Sin. B 8 (2018) 699–712, https://doi.org/10.1016/j.apsb.2018.05.005.

[8] S.C. Laizure, V. Herring, Z. Hu, K. Witbrodt, R.B. Parker, The role of human carboxylesterases in drug metabolism: have we overlooked their importance? Pharmacotherapy 33 (2013) 210–222, https://doi.org/10.1002/phar.1194.

[9] L. Di, The impact of carboxylesterases in drug metabolism and pharmacokinetics, Curr. Drug Metabol. 20 (2019) 91–102, https://doi.org/10.2174/1389200219666180821094502.

[10] J. Lian, R. Nelson, R. Lehner, Carboxylesterases in lipid metabolism: from mouse to human, Protein Cell 9 (2018) 178–195, https://doi.org/10.1007/s13238-017-0437-z.

[11] S. Mukherjee, M. Choi, J.W. Yun, Novel regulatory roles of carboxylesterase 3 in lipid metabolism and browning in 3T3-L1 white adipocytes, Appl. Physiol. Nutr. Metabol. (2019), https://doi.org/10.1139/apnm-2018-0814.

[12] L. Yang, X. Li, H. Tang, Z. Gao, K. Zhang, K. Sun, A unique role of carboxylesterase 3 (Ces3) in beta adrenergic signaling-stimulated thermogenesis, Diabetes 68 (2019) 1178–1196, https://doi.org/10.2337/db18-1210.

[13] R.S. Holmes, M.W. Wright, S.J. Laulederkind, L.A. Cox, M. Hosokawa, T. Imai, S. Ishibashi, R. Lehner, M. Miyazaki, E.J. Perkins, P.M. Potter, M.R. Redinbo, J. Robert, T. Satoh, T. Yamashita, B. Yan, T. Yokoi, R. Zechner, L.J. Maltais, Recommended nomenclature for five mammalian carboxylesterase gene families: human, mouse, and rat genes and proteins, Mamm. Genome 21 (2010) 427–441, https://doi.org/10.1007/s00335-010-9284-4.

[14] T. Imai, M. Hosokawa, Prodrug approach using carboxylesterases activity: catalytic properties and gene regulation of carboxylesterase in mammalian tissue, J. Pest. Sci. 35 (2010) 229–239, https://doi.org/10.1584/jpestics.R10-03.

[15] T. Imai, K. Ohura, The role of intestinal carboxylesterase in the oral absorption of prodrugs, Curr. Drug Metabol. 11 (2010) 793–805, https://doi.org/10.2174/138920010794328904.

[16] J. Rautio, N.A. Meanwell, L. Di, M.J. Hageman, The expanding role of prodrugs in contemporary drug design and development, Nat. Rev. Drug Discov. 17 (2018) 559–587, https://doi.org/10.1038/nrd.2018.46.

[17] T. Satoh, M. Hosokawa, Carboxylesterases: structure, function and polymorphism, Biomol Ther 17 (2009) 335–347, https://doi.org/10.4062/biomolther.2009.17.4.335.

[18] J.L. Staudinger, C. Xu, Y.J. Cui, C.D. Klaassen, Nuclear receptor-mediated regulation of carboxylesterase expression and activity, Expet Opin. Drug Metabol. Toxicol. 6 (2010) 261–271, https://doi.org/10.1517/17425250903483215.

[19] S.D. Varfolomeev, S.V. Lushchekina, A.V. Nemukhin, A.M. Kulakova, E.D. Kots, G.F. Makhaeva, H. Delacour, O. Lockridge, P. Masson, Molecular polymorphism of human enzymes as the basis of individual sensitivity to drugs. Supercomputer-assisted modeling as a tool for analysis of structural changes and enzymatic activity of proteins, Russ. Chem. Bull. 65 (2016) 1592–1607, https://doi.org/10.1007/s11172-016-1487-8.

[20] H.B. Rasmussen, D. Bjerre, K. Linnet, G. Jurgens, K. Dalhoff, H. Stefansson, T. Hankemeier, R. Kaddurah-Daouk, O. Taboureau, S. Brunak, T. Houmann, P. Jeppesen, A.K. Pagsberg, K. Plessen, J. Dyrborg, P.R. Hansen, P.E. Hansen, T. Hughes, T. Werge, I. Consortium, Individualization of treatments with drugs metabolized by CES1: combining genetics and metabolomics, Pharmacogenomics 16 (2015) 649–665, https://doi.org/10.2217/pgs.15.7.

[21] M. Neuvonen, E.K. Tarkiainen, A. Tornio, P. Hirvensalo, T. Tapaninen, M. Paile-Hyvarinen, M.K. Itkonen, M.T. Holmberg, V. Karja, V.T. Mannisto, P.J. Neuvonen, J. Pihlajamaki, J.T. Backman, M. Niemi, Effects of genetic variants on carboxylesterase 1 gene expression, and clopidogrel pharmacokinetics and antiplatelet effects, Basic Clin. Pharmacol. Toxicol. 122 (2018) 341–345, https://doi.org/10.1111/bcpt.12916.

[22] F. Chen, B. Zhang, R.B. Parker, S.C. Laizure, Clinical implications of genetic variation in carboxylesterase drug metabolism, Expet Opin. Drug Metabol. Toxicol. 14 (2018) 131–142, https://doi.org/10.1080/17425255.2018.1420164.

[23] X. Wang, J. Shi, H.J. Zhu, Functional study of carboxylesterase 1 protein isoforms, Proteomics 19 (2019), e1800288, https://doi.org/10.1002/pmic.201800288.

[24] S.C. Laizure, R.B. Parker, Is genetic variability in carboxylesterase-1 and carboxylesterase-2 drug metabolism an important component of personalized medicine? Xenobiotica 50 (2020) 92–100, https://doi.org/10.1080/00498254.2019.1678078.

[25] L. Her, H.J. Zhu, Carboxylesterase 1 and precision pharmacotherapy: pharmacogenetics and nongenetic regulators, Drug Metab. Dispos. 48 (2020) 230–244, https://doi.org/10.1124/dmd.119.089680.

[26] M.K. Ross, T.M. Streit, K.L. Herring, Carboxylesterases: dual roles in lipid and pesticide metabolism, J. Pestic. Sci. 35 (2010) 257–264, https://doi.org/10.1584/jpestics.R10-07.

[27] Z. Merali, S. Ross, G. Pare, The pharmacogenetics of carboxylesterases: CES1 and CES2 genetic variants and their clinical effect, Drug Metabol. Drug Interact. 29 (2014) 143–151, https://doi.org/10.1515/dmdi-2014-0009.

[28] Y. Xu, C. Zhang, W. He, D. Liu, Regulations of xenobiotics and endobiotics on carboxylesterases: a comprehensive review, Eur. J. Drug Metab. Pharmacokinet. 41 (2016) 321–330, https://doi.org/10.1007/s13318-016-0326-5.

[29] K.J. Yoon, J.L. Hyatt, C.L. Morton, R.E. Lee, P.M. Potter, M.K. Danks, Characterization of inhibitors of specific carboxylesterases: development of carboxylesterase inhibitors for translational application, Mol. Canc. Therapeut. 3 (2004) 903–909.

[30] M.R. Redinbo, P.M. Potter, Keynote review: mammalian carboxylesterases: from drug targets to protein therapeutics, Drug Discov. Today 10 (2005) 313–325, https://doi.org/10.1016/s1359-6446(05)03383-0.
[31] M.J. Hatfield, P.M. Potter, Carboxylesterase inhibitors, Expert Opin. Ther. Pat. 21 (2011) 1159–1171, https://doi.org/10.1517/13543776.2011.586339.
[32] D.D. Wang, L.W. Zou, Q. Jin, J. Hou, G.B. Ge, L. Yang, Recent progress in the discovery of natural inhibitors against human carboxylesterases, Fitoterapia 117 (2017) 84–95, https://doi.org/10.1016/j.fitote.2017.01.010.
[33] L.W. Zou, Q. Jin, D.D. Wang, Q.K. Qian, D.C. Hao, G.B. Ge, L. Yang, Carboxylesterase inhibitors: an update, Curr. Med. Chem. 25 (2018) 1627–1649, https://doi.org/10.2174/0929867325666171204155558.
[34] R.M. Wadkins, J.L. Hyatt, K.J. Yoon, C.L. Morton, R.E. Lee, K. Damodaran, P. Beroza, M.K. Danks, P.M. Potter, Discovery of novel selective inhibitors of human intestinal carboxylesterase for the amelioration of irinotecan-induced diarrhea: synthesis, quantitative structure-activity relationship analysis, and biological activity, Mol. Pharmacol. 65 (2004) 1336–1343, https://doi.org/10.1124/mol.65.6.1336.
[35] R.M. Wadkins, J.L. Hyatt, X. Wei, K.J. Yoon, M. Wierdl, C.C. Edwards, C.L. Morton, J.C. Obenauer, K. Damodaran, P. Beroza, M.K. Danks, P.M. Potter, Identification and characterization of novel benzil (diphenylethane-1,2-dione) analogues as inhibitors of mammalian carboxylesterases, J. Med. Chem. 48 (2005) 2906–2915, https://doi.org/10.1021/jm049011j.
[36] E.I. Parkinson, M. Jason Hatfield, L. Tsurkan, J.L. Hyatt, C.C. Edwards, L.D. Hicks, B. Yan, P.M. Potter, Requirements for mammalian carboxylesterase inhibition by substituted ethane-1,2-diones, Bioorg. Med. Chem. 19 (2011) 4635–4643, https://doi.org/10.1016/j.bmc.2011.06.012.
[37] J.L. Hyatt, T. Moak, M.J. Hatfield, L. Tsurkan, C.C. Edwards, M. Wierdl, M.K. Danks, R.M. Wadkins, P.M. Potter, Selective inhibition of carboxylesterases by isatins, indole-2,3-diones, J. Med. Chem. 50 (2007) 1876–1885, https://doi.org/10.1021/jm061471k.
[38] M.J. McKay, A.R. Carroll, R.J. Quinn, J.N.A. Hooper, 1,2-Bis(1H-indol-3-yl) ethane-1,2-dione, an indole alkaloid from the marine sponge *Smenospongia* sp, J. Nat. Prod. 65 (2002) 595–597, https://doi.org/10.1021/np010347v.
[39] M.J. Hatfield, L.G. Tsurkan, J.L. Hyatt, C.C. Edwards, A. Lemoff, C. Jeffries, B. Yan, P.M. Potter, Modulation of esterified drug metabolism by tanshinones from Salvia miltiorrhiza ("Danshen"), J. Nat. Prod. 76 (2013) 36–44, https://doi.org/10.1021/np300628a.
[40] M.J. Hatfield, J. Chen, E.M. Fratt, L. Chi, J.C. Bollinger, R.J. Binder, J. Bowling, J.L. Hyatt, J. Scarborough, C. Jeffries, P.M. Potter, Selective inhibitors of human liver carboxylesterase based on a beta-lapachone scaffold: novel reagents for reaction profiling, J. Med. Chem. 60 (2017) 1568–1579, https://doi.org/10.1021/acs.jmedchem.6b01849.
[41] C.E. Wheelock, T.F. Severson, B.D. Hammock, Synthesis of new carboxylesterase inhibitors and evaluation of potency and water solubility, Chem. Res. Toxicol. 14 (2001) 1563–1572, https://doi.org/10.1021/tx015508+.
[42] G.R. Mukhamadieva, N.P. Boltneva, T.G. Galenko, V.B. Sokolov, T.A. Epishina, G.F. Makhaeva, Synthesis and biological activity of O-carbamoylated 1,1,1,3,3,3-hexafluoroisopropanols as new specific inhibitors of carboxylesterase, Pharm. Chem. J. 46 (2012) 461–464, https://doi.org/10.1007/s11094-012-0825-x.
[43] E. Dominguez, A. Galmozzi, J.W. Chang, K.L. Hsu, J. Pawlak, W. Li, C. Godio, J. Thomas, D. Partida, S. Niessen, P.E. O'Brien, A.P. Russell, M.J. Watt, D.K. Nomura, B.F. Cravatt, E. Saez, Integrated phenotypic and activity-based profiling links Ces3 to obesity and diabetes, Nat. Chem. Biol. 10 (2014) 113–121, https://doi.org/10.1038/nchembio.1429.
[44] J.L. Hyatt, R.M. Wadkins, L. Tsurkan, L.D. Hicks, M.J. Hatfield, C.C. Edwards, C.R. Ross 2nd, S.A. Cantalupo, G. Crundwell, M.K. Danks, R.K. Guy, P.M. Potter, Planarity and constraint of the carbonyl groups in 1,2-diones are determinants for selective inhibition of human carboxylesterase 1, J. Med. Chem. 50 (2007) 5727–5734, https://doi.org/10.1021/jm0706867.
[45] M.J. Hatfield, L. Tsurkan, M. Garrett, T.M. Shaver, J.L. Hyatt, C.C. Edwards, L.D. Hicks, P.M. Potter, Organ-specific carboxylesterase profiling identifies the small intestine and kidney as major contributors of activation of the anticancer prodrug CPT-11, Biochem. Pharmacol. 81 (2011) 24–31, https://doi.org/10.1016/j.bcp.2010.09.001.
[46] R.M. Wadkins, J.L. Hyatt, C.C. Edwards, L. Tsurkan, M.R. Redinbo, C.E. Wheelock, P.D. Jones, B.D. Hammock, P.M. Potter, Analysis of mammalian carboxylesterase inhibition by trifluoromethylketone-containing compounds, Mol. Pharmacol. 71 (2007) 713–723, https://doi.org/10.1124/mol.105.021683.
[47] A.A. Székács, B. Bordás, B.D. Hammock, Transition state analog enzyme inhibitors: structure-activity relationships of trifluoromethyl ketones, in: D. W, F. T (Eds.), Rational Approaches to Structure, Activity, and Ecotoxicology of Agrochemicals, CRC Press, Boca Raton, Florida, 1992, pp. 219–249.
[48] I.V. Zueva, S.V. Lushchekina, I.R. Pottie, S. Darvesh, P. Masson, 1-(3-Tert-Butylphenyl)-2,2,2-Trifluoroethanone as a potent transition-state analogue slow-binding inhibitor of human acetylcholinesterase: kinetic, MD and QM/MM studies, Biomolecules 10 (2020) 1608, https://doi.org/10.3390/biom10121608.
[49] T. Harada, Y. Nakagawa, R.M. Wadkins, P.M. Potter, C.E. Wheelock, Comparison of benzil and trifluoromethyl ketone (TFK)-mediated carboxylesterase inhibition using classical and 3D-quantitative structure-activity relationship analysis, Bioorg. Med. Chem. 17 (2009) 149–164, https://doi.org/10.1016/j.bmc.2008.11.008.
[50] M. Harel, D.M. Quinn, H.K. Nair, I. Silman, J.L. Sussman, The X-ray structure of a transition state analog complex reveals the molecular origins of the catalytic power and substrate specificity of acetylcholinesterase, J. Am. Chem. Soc. 118 (1996) 2340–2346, https://doi.org/10.1021/ja952232h.
[51] Y. Zhang, J. Kua, J.A. McCammon, Role of the catalytic triad and oxyanion hole in acetylcholinesterase catalysis: an ab initio QM/MM study, J. Am. Chem. Soc. 124 (2002) 10572–10577, https://doi.org/10.1021/ja020243m.
[52] P.D. Ngo, S.O. Mansoorabadi, P.A. Frey, Serine protease catalysis: a computational study of tetrahedral intermediates and inhibitory adducts, J. Phys. Chem. B 120 (2016) 7353–7359, https://doi.org/10.1021/acs.jpcb.6b04089.
[53] N.P. Boltneva, G.F. Makhaeva, N.V. Kovaleva, S.V. Lushchekina, Y.V. Burgart, E.V. Shchegol'kov, V.I. Saloutin, O.N. Chupakhin, Alkyl 2-arylhydrazinylidene-3-oxo-3-polyfluoroalkylpropionates as new effective and selective inhibitors of carboxylesterase, Dokl. Biochem. Biophys. 465 (2015) 381–385, https://doi.org/10.1134/S1607672915060101.
[54] N.P. Boltneva, G.F. Makhaeva, E.V. Shchegol'kov, Y.V. Burgart, V.I. Saloutin, Selective carboxylesterase inhibitors for improving efficacy, safety and rational use of ester-containing drugs, Biomed Chem Res Meth 1 (2018), e00026, https://doi.org/10.18097/bmcrm00026.
[55] G.F. Makhaeva, E.V. Rudakova, N.V. Kovaleva, S.V. Lushchekina, N.P. Boltneva, A.N. Proshin, E.V. Shchegolkov, Y.V. Burgart, V.I. Saloutin, Cholinesterase and carboxylesterase inhibitors as pharmacological agents, Russ. Chem. Bull. 68 (2019) 967–984, https://doi.org/10.1007/s11172-019-2507-2.
[56] G.F. Makhaeva, N.A. Elkina, E.V. Shchegolkov, N.P. Boltneva, S.V. Lushchekina, O.G. Serebryakova, E.V. Rudakova, N.V. Kovaleva, E.V. Radchenko, V.V. Palyulin, Y.V. Burgart, V.I. Saloutin, S.O. Bachurin, R.J. Richardson, Synthesis, molecular docking, and biological evaluation of 3–oxo–2–tolylhydrazinylidene-4,4,4-trifluorobutanoates bearing higher and natural alcohol moieties as new selective carboxylesterase inhibitors, Bioorg. Chem. (2019) 103097, https://doi.org/10.1016/j.bioorg.2019.103097.
[57] O.G. Khudina, G.F. Makhaeva, N.A. Elkina, N.P. Boltneva, O.G. Serebryakova, E.V. Shchegolkov, E.V. Rudakova, S.V. Lushchekina, Y.V. Burgart, S.O. Bachurin, R.J. Richardson, V.I. Saloutin, Synthesis of 2-arylhydrazinylidene-3-oxo-4,4,4-trifluorobutanoic acids as new selective carboxylesterase inhibitors and radical scavengers, Bioorg. Med. Chem. Lett (2019) 126716, https://doi.org/10.1016/j.bmcl.2019.126716.
[58] E.V. Shchegol'kov, G.F. Makhaeva, N.P. Boltneva, S.V. Lushchekina, O.G. Serebryakova, E.V. Rudakova, N.V. Kovaleva, Y.V. Burgart, V.I. Saloutin, O.N. Chupakhin, S.O. Bachurin, R.J. Richardson, Synthesis, molecular docking, and biological activity of polyfluoroalkyl dihydroazolo[5,1-c][1,2,4]triazines as selective carboxylesterase inhibitors, Bioorg. Med. Chem. 25 (2017) 3997–4007, https://doi.org/10.1016/j.bmc.2017.05.045.
[59] P. Sharma, A. Kumar, M. Sharma, J. Singh, P. Bandyopadhyay, M. Sathe, M.P. Kaushik, Synthesis and exploration of QSAR model of 2-methyl-3-[2-(2-methylprop-1-en-1-yl)-1H-benzimidazol-1-yl]pyrimido[1,2-a]benzim idazol-4(3H)-one as potential antibacterial agents, J. Enzym. Inhib. Med. Chem. 27 (2012) 294–301, https://doi.org/10.3109/14756366.2011.587814.
[60] P. Bandyopadhyay, L. Guha, T. Seenivasagan, M. Sathe, P. Sharma, B.D. Parashar, M.P. Kaushik, Synthesis and bio-evaluation of aryl hydrazono esters for oviposition responses in Aedes albopictus, Bioorg. Med. Chem. Lett. 21 (2011) 794–797, https://doi.org/10.1016/j.bmcl.2010.11.101.
[61] X. Zhu, Y. Chen, Y. Chen, J. Wang, W. Su, Mechanically activated solid-state synthesis of phenylhydrazone derivatives via high-speed ball milling, Lett. Org. Chem. 11 (2014) 621–626, https://doi.org/10.2174/15701786119991404041114 11.
[62] C. Liu, J. Lv, S. Luo, J.P. Cheng, Sc(OTf)3-catalyzed transfer diazenylation of 1,3-dicarbonyls with triazenes via N-N bond cleavage, Org. Lett. 16 (2014) 5458–5461, https://doi.org/10.1021/ol5027014.
[63] V.I. Filyakova, N.S. Karpenko, O.A. Kuznetsova, K.I. Pashkevich, New fluorinated synthons: lithium salts derived from fluorinated β-diketones, Russ. J. Org. Chem. 34 (1998) 381–387.
[64] O.G. Khudina, E.V. Shchegol'kov, Y.V. Burgart, V.I. Saloutin, O.N. Chupakhin, The interaction of fluorinated 2-arylhydrazono-1,3-dicarbonyl compounds with o-phenylenediamine, J. Fluor. Chem. 125 (2004) 1363–1370, https://doi.org/10.1016/j.jfluchem.2004.04.004.
[65] O.G. Khudina, E.V. Shchegol'kov, Y.V. Burgart, M.I. Kodess, V.I. Saloutin, O.N. Chupakhin, Recyclization of 7-fluoroalkyl-4,7-dihydroazolo[5,1-c]triazines into 5-(Pyrazolinylhydrazono)azoles in the reactions with hydrazides and thiosemicarbazide, Heterocycles 68 (2006) 2515–2525, https://doi.org/10.3987/COM-06-10877.
[66] Y.V. Burgart, A.S. Fokin, O.G. Kuzueva, O.N. Chupakhin, V.I. Saloutin, Synthesis of fluorinated 2(3)-arylhydrazones of 1,2,3-tri(1,2,3,4-tetra)carbonyl compounds and their heterocyclization reactions, J. Fluor. Chem. 92 (1998) 101–108, https://doi.org/10.1016/s0022-1139(98)00247-4.
[67] O.G. Khudina, Y.V. Burgart, E.V. Shchegol'kov, V.I. Saloutin, O.N. Kazheva, A.N. Chekhlov, O.A. D'yachenko, Steric structure of alkyl 2-aryl(hetaryl) hydrazono-3-fluoroalkyl-3-oxopropionates, Russ. J. Org. Chem. 45 (2009) 801–809, https://doi.org/10.1134/s1070428009060013.
[68] G.F. Makhaeva, E.V. Radchenko, V.A. Palyulin, E.V. Rudakova, A.Y. Aksinenko, V.B. Sokolov, N.S. Zefirov, R.J. Richardson, Organophosphorus compound esterase profiles as predictors of therapeutic and toxic effects, Chem. Biol. Interact. 203 (2013) 231–237, https://doi.org/10.1016/j.cbi.2012.10.012.
[69] G.F. Makhaeva, N.P. Boltneva, S.V. Lushchekina, O.G. Serebryakova, T.S. Stupina, A.A. Terentiev, I.V. Serkov, A.N. Proshin, S.O. Bachurin, R.J. Richardson, Synthesis, molecular docking and biological evaluation of N,N-disubstituted 2-aminothiazolines as a new class of

butyrylcholinesterase and carboxylesterase inhibitors, Bioorg. Med. Chem. 24 (2016) 1050–1062, https://doi.org/10.1016/j.bmc.2016.01.031.
[70] G.F. Makhaeva, E.V. Rudakova, O.G. Serebryakova, A.Y. Aksinenko, S.V. Lushchekina, S.O. Bachurin, R.J. Richardson, Esterase profiles of organophosphorus compounds in vitro predict their behavior in vivo, Chem. Biol. Interact. 259 (2016) 332–342, https://doi.org/10.1016/j.cbi.2016.05.002.
[71] G.M. Morris, R. Huey, W. Lindstrom, M.F. Sanner, R.K. Belew, D.S. Goodsell, A.J. Olson, AutoDock4 and AutoDockTools4: automated docking with selective receptor flexibility, J. Comput. Chem. 30 (2009) 2785–2791, https://doi.org/10.1002/jcc.21256.
[72] A. Parkinson, B.W. Ogilvie, D.B. Buckley, F. Kazmi, M. Czerwinski, O. Parkinson, Biotransformation of xenobiotics, in: C.D. Klaassen, J.B. Watkins III (Eds.), Casarett & Doull's Essentials of Toxicology, The McGraw-Hill Companies, Inc, New York, 2015, pp. 79–107.
[73] L. Hedges, S. Brown, A.K. MacLeod, A. Vardy, E. Doyle, G. Song, M. Moreau, M. Yoon, T.G. Osimitz, B.G. Lake, Metabolism of deltamethrin and cis- and trans-permethrin by human expressed cytochrome P450 and carboxylesterase enzymes, Xenobiotica 49 (2019) 521–527, https://doi.org/10.1080/00498254.2018.1474283.
[74] L.A. Videla, Oxidative stress signaling underlying liver disease and hepatoprotective mechanisms, World J. Hepatol. 1 (2009) 72–78, https://doi.org/10.4254/wjh.v1.i1.72.
[75] G.A. de la Riva, F.J. Lopez Mendoza, G. Aguero-Chapin, Known hepatoprotectors act as antioxidants and immune stimulators in stressed mice: perspectives in animal health care, Curr. Pharmaceut. Des. 24 (2018) 4825–4837, https://doi.org/10.2174/1381612825666190116151628.
[76] R. Re, N. Pellegrini, A. Proteggente, A. Pannala, M. Yang, C. Rice-Evans, Antioxidant activity applying an improved ABTS radical cation decolorization assay, Free Radic. Biol. Med. 26 (1999) 1231–1237, https://doi.org/10.1016/s0891-5849(98)00315-3.
[77] A. Mitchell, D.C. Nonhebel, Spectroscopic studies of tautomeric systems—III, Tetrahedron 35 (1979) 2013–2019, https://doi.org/10.1016/s0040-4020(01)88971-7.
[78] O.G. Kuzueva, Y.V. Burgart, V.I. Saloutin, Synthesis of 2-arylhydrazones of aliphatic fluorine-containing 1,2,3-tricarbonyl compounds and their reactions with dinucleophiles, Russ. Chem. Bull. 47 (1998) 673–678, https://doi.org/10.1007/bf02495977.
[79] O.G. Khudina, E.V. Shchegol'kov, Y.V. Burgart, M.I. Kodess, V.I. Saloutin, O.N. Kazheva, G.V. Shilov, O.A. D'yachenko, M.A. Grishina, V.A. Potemkin, O.N. Chupakhin, Geometric isomerism in the series of fluoroalkyl-containing 1,2,3-trione 2-arylhydrazones, Russ. J. Org. Chem. 43 (2007) 380–387, https://doi.org/10.1134/s1070428007030086.
[80] S.H. Sterri, B.A. Johnsen, F. Fonnum, A radiochemical assay method for carboxylesterase, and comparison of enzyme activity towards the substrates methyl [1-14C] butyrate and 4-nitrophenyl butyrate, Biochem. Pharmacol. 34 (1985) 2779–2785, https://doi.org/10.1016/0006-2952(85)90579-9.
[81] G.L. Ellman, K.D. Courtney, V. Andres, R.M. Featherstone, A new and rapid colorimetric determination of acetylcholinesterase activity, Biochem. Pharmacol. 7 (1961) 88–95, https://doi.org/10.1016/0006-2952(61)90145-9.
[82] T.A. Krylova, A.M. Kol'tsova, V.V. Zenin, A.S. Musorina, T.K. Iakovleva, G.G. Polianskaia, [Comparative characteristics of new mesenchymal stem cell lines derived from human embryonic stem cells, bone marrow and foreskin], Tsitologiia 54 (2012) 5–16 [In Russian].
[83] T. Mosmann, Rapid colorimetric assay for cellular growth and survival: application to proliferation and cytotoxicity assays, J. Immunol. Methods 65 (1983) 55–63, https://doi.org/10.1016/0022-1759(83)90303-4.
[84] On Circulation of Medicines, Federal Law of 12.04.2010. №61-FZ RF.
[85] A.N. Mironov, Guidelines for Pre-clinical Study of Medicinal Products, Grif&Ko, Moscow, 2012 (in Russian).
[86] OECD Guideline 423. Acute Oral Toxicity, OECD, Paris, 1996.
[87] M.W. Schmidt, K. Baldridge, J. Boatz, S. Elbert, M.S. Gordon, J.H. Jenson, S. Koseki, N. Matsunaga, K.A. Nguyen, S.J. Su, T.L. Windus, M. Dupuis, J. Montgomery, General Atomic and Molecular Electronic Structure System, 1993.
[88] S. Bencharit, C.C. Edwards, C.L. Morton, E.L. Howard-Williams, P. Kuhn, P.M. Potter, M.R. Redinbo, Multisite promiscuity in the processing of endogenous substrates by human carboxylesterase 1, J. Mol. Biol. 363 (2006) 201–214, https://doi.org/10.1016/j.jmb.2006.08.025.
[89] J. Cheung, M.J. Rudolph, F. Burshteyn, M.S. Cassidy, E.N. Gary, J. Love, M.C. Franklin, J.J. Height, Structures of human acetylcholinesterase in complex with pharmacologically important ligands, J. Med. Chem. 55 (2012) 10282–10286, https://doi.org/10.1021/jm300871x.
[90] Y. Nicolet, O. Lockridge, P. Masson, J.C. Fontecilla-Camps, F. Nachon, Crystal structure of human butyrylcholinesterase and of its complexes with substrate and products, J. Biol. Chem. 278 (2003) 41141–41147, https://doi.org/10.1074/jbc.M210241200.
[91] P. Masson, S. Lushchekina, L.M. Schopfer, O. Lockridge, Effects of viscosity and osmotic stress on the reaction of human butyrylcholinesterase with cresyl saligenin phosphate, a toxicant related to aerotoxic syndrome: kinetic and molecular dynamics studies, Biochem. J. 454 (2013) 387–399, https://doi.org/10.1042/bj20130389.
[92] J.M. Word, S.C. Lovell, J.S. Richardson, D.C. Richardson, Asparagine and glutamine: using hydrogen atom contacts in the choice of side-chain amide orientation, J. Mol. Biol. 285 (1999) 1735–1747, https://doi.org/10.1006/jmbi.1998.2401.
[93] P.-O. Löwdin, On the nonorthogonality problem, in: L. Per-Olov (Ed.), Advances in Quantum Chemistry, Academic Press, 1970, pp. 185–199.
[94] S.V. Lushchekina, G.F. Makhaeva, D.A. Novichkova, I.V. Zueva, N.V. Kovaleva, R.J. Richardson, Supercomputer modeling of dual-site acetylcholinesterase (AChE) inhibition, JSFI 5 (2018) 89–97, https://doi.org/10.14529/jsfi1804.
[95] G.M. Morris, D.S. Goodsell, R.S. Halliday, R. Huey, W.E. Hart, R.K. Belew, A.J. Olson, Automated docking using a Lamarckian genetic algorithm and an empirical binding free energy function, J. Comput. Chem. 19 (1998) 1639–1662, https://doi.org/10.1002/(sici)1096-987x(19981115)19:14<1639::aid-jcc10>3.0.co;2-b.
[96] E.V. Radchenko, A.S. Dyabina, V.A. Palyulin, N.S. Zefirov, Prediction of human intestinal absorption of drug compounds, Russ. Chem. Bull. 65 (2) (2016) 576–580, https://doi.org/10.1007/s11172-016-1340-0.
[97] A.S. Dyabina, E.V. Radchenko, V.A. Palyulin, N.S. Zefirov, Prediction of blood-brain barrier permeability of organic compounds, Dokl. Biochem. Biophys. 470 (2016) 371–374, https://doi.org/10.1134/S1607672916050173.
[98] E.V. Radchenko, Y.A. Rulev, A.Y. Safanyaev, V.A. Palyulin, N.S. Zefirov, Computer-aided estimation of the hERG-mediated cardiotoxicity risk of potential drug components, Dokl. Biochem. Biophys. 473 (2017) 128–131, https://doi.org/10.1134/S1607672917020107.
[99] ADMET prediction service. http://qsar.chem.msu.ru/admet/. Accessed Dec 01, 2020.
[100] I. Sushko, S. Novotarskyi, R. Korner, A.K. Pandey, M. Rupp, W. Teetz, S. Brandmaier, A. Abdelaziz, V.V. Prokopenko, V.Y. Tanchuk, R. Todeschini, A. Varnek, G. Marcou, P. Ertl, V. Potemkin, M. Grishina, J. Gasteiger, C. Schwab, Baskin II, V.A. Palyulin, E.V. Radchenko, W.J. Welsh, V. Kholodovych, D. Chekmarev, A. Cherkasov, J. Aires-de-Sousa, Q.Y. Zhang, A. Bender, F. Nigsch, L. Patiny, A. Williams, V. Tkachenko, I.V. Tetko, Online chemical modeling environment (OCHEM): web platform for data storage, model development and publishing of chemical information, J. Comput. Aided Mol. Des. 25 (2011) 533–554, https://doi.org/10.1007/s10822-011-9440-2.
[101] G.R. Bickerton, G.V. Paolini, J. Besnard, S. Muresan, A.L. Hopkins, Quantifying the chemical beauty of drugs, Nat. Chem. 4 (2012) 90–98, https://doi.org/10.1038/nchem.1243.
[102] RDKit: open-source cheminformatics software. http://www.rdkit.org. (Accessed 1 February 2021).
[103] V. Voevodin, A. Antonov, D. Nikitenko, P. Shvets, S. Sobolev, I. Sidorov, K. Stefanov, V. Voevodin, S. Zhumatiy, Supercomputer Lomonosov-2: large scale, deep monitoring and fine analytics for the user community, JSFI 6 (2019) 4–11, https://doi.org/10.14529/jsfi190201.